AN EXPERIMENTAL INVESTIGATION OF THE HEAT TRANSFER FROM A BUOYANT GAS PLUME TO A HORIZONTAL UNOBSTRUCTED CEILING

Thesis by

Charl Christo Veldman

In Partial Fulfillment of the Requirements

For the Degree of

Mechanical Engineer

California Institute of Technology

Pasadena, California

1975

(Submitted May 2, 1975)

ACKNOWLEDGMENTS

The author wishes to express his gratitude to Professor E. Zukoski for his guidance and encouragement during the course of this investigation. The information and ideas obtained through discussions with Professors R. Sabersky and T. Kubota are also deeply appreciated. Most of the experimental work was performed with the assistance of Mr. Barry Schneidman and in part that of Mr. F. T. Linton, whose efforts are gratefully acknowledged. A word of thanks is owed to Roberta Duffy for the expert typing of this thesis.

This work was sponsored by the Engineering Division of the California Institute of Technology and in part by a National Bureau of Standards contract, to whom the author is thankful. Finally, the author wishes to express his gratitude to the South African Council for Scientific and Industrial Research, who granted a scholarship for two years of graduate study at this Institute.

This work is dedicated to my wife, Christel, whose confidence and understanding made it possible; and to my parents, in appreciation for their inspiration.

ABSTRACT

This thesis presents an experimental investigation of the axisymmetric heat transfer from a small scale fire and resulting buoyant plume to a horizontal, unobstructed ceiling during the initial stages of development. A propane-air burner yielding a heat source strength between 1.0 kW and 1.6 kW was used to simulate the fire, and measurements proved that this heat source did satisfactorily represent a source of buoyancy only. The ceiling consisted of a 1/16" steel plate of 0.91 m diameter, insulated on the upper side. The ceiling height was adjustable between 0.5 m and 0.91 m. Temperature measurements were carried out in the plume, ceiling jet, and on the ceiling.

Heat transfer data were obtained by using the transient method and applying corrections for the radial conduction along the ceiling and losses through the insulation material. The ceiling heat transfer coefficient was based on the adiabatic ceiling jet temperature (recovery temperature) reached after a long time. A parameter involving the source strength Q and ceiling height H was found to correlate measurements of this temperature and its radial variation. A similar parameter for estimating the ceiling heat transfer coefficient was confirmed by the experimental results.

This investigation therefore provides reasonable estimates for the heat transfer from a buoyant gas plume to a ceiling in the axisymmetric case, for the stagnation region where such heat transfer is a maximum and for the ceiling jet region ($r/H \leq 0.7$). A comparison with data from experiments which involved larger heat sources indi-

cates that the predicted scaling of temperatures and heat transfer rates for larger scale fires is adequate.

TABLE OF CONTENTS

LIST OF SYMBOLS

A	area (m^2)
b	plume Gaussian width (m)
B	initial buoyancy flux (m^4/s^3)
C, C_p	specific heat ($Ws/kg\ ^oK$)
D	nozzle diameter (m)
ΔE	increase in ceiling internal energy (W/m^2)
f	friction factor
f_1	dimensionless function of r/H ; see p. 18, eqn. (2.29)
f_2	dimensionless function of r/H ; see p. 31, eqn. (2.52)
g	acceleration of gravity (m/s^2)
h	heat transfer coefficient ($W/m^2\ ^oK$)
h_c'	dimensionless heat transfer coefficient, see p. 31
H	ceiling height (m)
k	conductivity ($W/m\ ^oK$)
ℓ	ceiling jet Gaussian width (m)
$\dot{m}$	mass flow rate (kg/s)
m	momentum flux (m^4/s^2)
M	initial momentum flux (m^4/s^2)
Δp	pressure gradient (N/m^2)
Pr	Prandtl number
q	heat transfer/unit area (W/m^2)
Q	heat source strength (W)
$\dot{Q}$	initial volume flux (m^3/s)
Q^*	dimensionless heat addition parameter, $Q/\rho_\infty C_p T_\infty \sqrt{gz}\, z^2$
r	radius (m)

Re	Reynolds number
St	Stanton number
T	temperature (^{o}K or ^{o}C)
T^*	$T_\infty (Q^*)^{2/3}$
ΔT	$(T-T_\infty)$
u, V	velocity (m/s)
y	ceiling jet vertical dimension (m)
z	vertical dimension from heat source (m)
β	coefficient of expansion (gas) ($1/^{o}$K)
$\dot{\beta}$	kinematic buoyancy flux (m^4/s^3)
δ	ceiling thickness (m)
μ	dynamic viscosity (kg/ms)
$\dot{\mu}$	volume flux (m^3/s)
$\varkappa$	thermal diffusivity (m^2/s)
ρ	density (kg/m^3)

Subscripts

ad	adiabatic; see Section II. E. 2, p. 28 ff.
c	ceiling
g	ceiling jet
max	maximum value in plume or ceiling jet
p	plume
0, ∞	ambient

I. INTRODUCTION

The heat transfer from a buoyant plume of hot gas rising above a fire to a horizontal ceiling has, in recent years, drawn the attention of several researchers. The understanding of this phenomenon will be of great help in estimating the magnitudes of heat transfer in the developing stages of fires in buildings. If, e.g., the heat transfer rate to a ceiling could be reduced by 50 per cent, the fire department would have effectively double the time in which to react, and this should result in a considerable reduction in damage. Heat transfer to a ceiling is also very important in estimating the optimum placement of fire detectors in buildings[1].

The experimental study reported in this thesis was primarily concerned with estimating the heat transfer rate from an axisymmetric buoyant plume of hot gas rising above a single heat source to a horizontal unobstructed ceiling. Since the experimental determination of heat transfer is not a trivial problem, this investigation was aimed at obtaining an order of magnitude of such heat transfer rates and coefficients as a function of radius along the ceiling, rather than trying to develop a sophisticated technique to increase the accuracy of such measurements.

All measurements of heat transfer were of a transient nature and attention was focussed on the first 7 minutes after the fire was started. The actual heat transfer rates were obtained from the increase in internal energy of the ceiling, after application of correction factors for heat losses due to conduction along the ceiling and from the upper surface of the ceiling.

Temperature measurements were also carried out in the buoyant plume (without the ceiling) and in the ceiling jet for comparison with results obtained by several other researchers.

In order to investigate the agreement with theoretical predictions, two different heat source strengths (1.17 kW and 1.53 kW) were used with two different geometrical configurations (ceiling heights of 59 cm and 81 cm above the source).

This experimental investigation, however, also posed various limitations, the elimination of which will be of great help in obtaining a clearer understanding of the ceiling heat transfer process. The most important limitation was the absence of any velocity measurements in the plume as well as in the ceiling jet, due to the fact that relatively large temperature fluctuations prevented the use of an ordinary hot wire anemometer. Temperature compensation, or other sophisticated techniques for velocity measurements, were required. Such instruments were not available during these experiments, as the result of a time limitation.

Taking these limitations into account, this investigation yielded interesting and applicable results, and also provided a number of suggestions for a more detailed study of the ceiling heat transfer from a floor-level fire.

II. EXPERIMENTAL AND ANALYTICAL MODEL

A. General Description

The experimental investigation of the heat transfer from a buoyant plume to a horizontal unobstructed ceiling required the development of an experimental model that would make possible such heat transfer and temperature measurements. The following basic requirements existed:

i) a heat source capable of generating an axisymmetric buoyant plume similar to that generated by a real floor-level fire; and ii) a ceiling on which temperature and heat transfer measurements can be carried out with reasonable accuracy.

Such a heat transfer model therefore consisted of the following "components:" a) heat source, b) buoyant plume, c) ceiling jet and turning region, d) ceiling. Each of these "components" is treated separately in the following sections.

In deciding on the basic dimensions for ceiling height and diameter, it was attempted to scale to some degree the geometric proportions of an average room. Being one of the major parameters in this model, the ceiling height H was adjustable between 0.5 m and 0.9 m. A ceiling with a diameter of approximately 0.9 m was selected to give a height-to-radius ratio near one.

The other major parameter governing the ceiling heat transfer, the strength of the heat source Q, had to be adjustable too. It was decided to utilize a heat source that would yield values of Q between 1.0 and 1.5 kW.

A schematic diagram of the experimental model outlined above is shown in Figure 1.

The experiments were conducted in a room of dimensions 7.2 m × 6.0 m with a ceiling height of 3.4 m. All doors and ventilation ducts were sealed to prevent any externally-induced motion of the ambient air. Considerable time was allowed for the environment to become steady after entering the room and before each experiment was started.

B. Heat Source

Different kinds of heat sources were experimented with, in order to find the most suitable source that would meet the following requirements:

i) produce a stable and steady axisymmetric buoyant plume;

ii) have negligible momentum flux compared to the buoyancy flux (in order to simulate a floor-level fire);

(iii) provide a simple though reasonably accurate method of determining the heat released, i.e., the source strength;

iv) source strength must be adjustable to produce from 1 kW to 1.5 kW.

As a first attempt, alcohol (denatured ethanol) was poured into a pyrex glass beaker and the surface was lit. The resulting diffusive flame was very unstable and had the tendency to "wander" around, resulting in a very unstable plume. Heat sources of this type were used by Yokoi[2] in a study of buoyant plumes above point heat sources and heat sources of finite radius.

In an attempt to stabilize the resulting diffusive flame, a strip of asbestos fiber was rolled in a spiral and placed in the beaker of alcohol to serve as a wick. Capillary action through the asbestos produced an ample supply of alcohol for combustion. Though this resulted in a slightly less "wandering" flame, the plume still seemed to be fairly unstable. A further disadvantage of this type of heat source is that the alcohol has to be kept at a constant level and the amount of alcohol consumed has to be measured in order to calculate the source strength.

Another type of heat source which was considered was using an electrical heating element in a duct over which a known flow rate of air can be blown. This method proved not to be very attractive because of a large amount of radiant heat flux.

It was then decided to use a propane-air burner to produce the desired buoyant plume. Such a burner was constructed at almost no cost, and it had the added advantage that by just measuring the volumetric flow rate of propane and using the heating value, the source strength can be calculated to a reasonable degree of accuracy, assuming that enough air is supplied to ensure a stoichiometric or slightly lean flame (see Appendix A). A schematic layout of this burner is given below. Two Fisher-Porter rotameter flowmeters were used to meter the gas and air flow rates. These flowmeters were calibrated for air and propane flows, respectively.

The dimensions of the burner were determined by the source strength (Q) and the initial momentum flux (M), which had to be kept as low as possible. Since the source strength fixed the mass flow

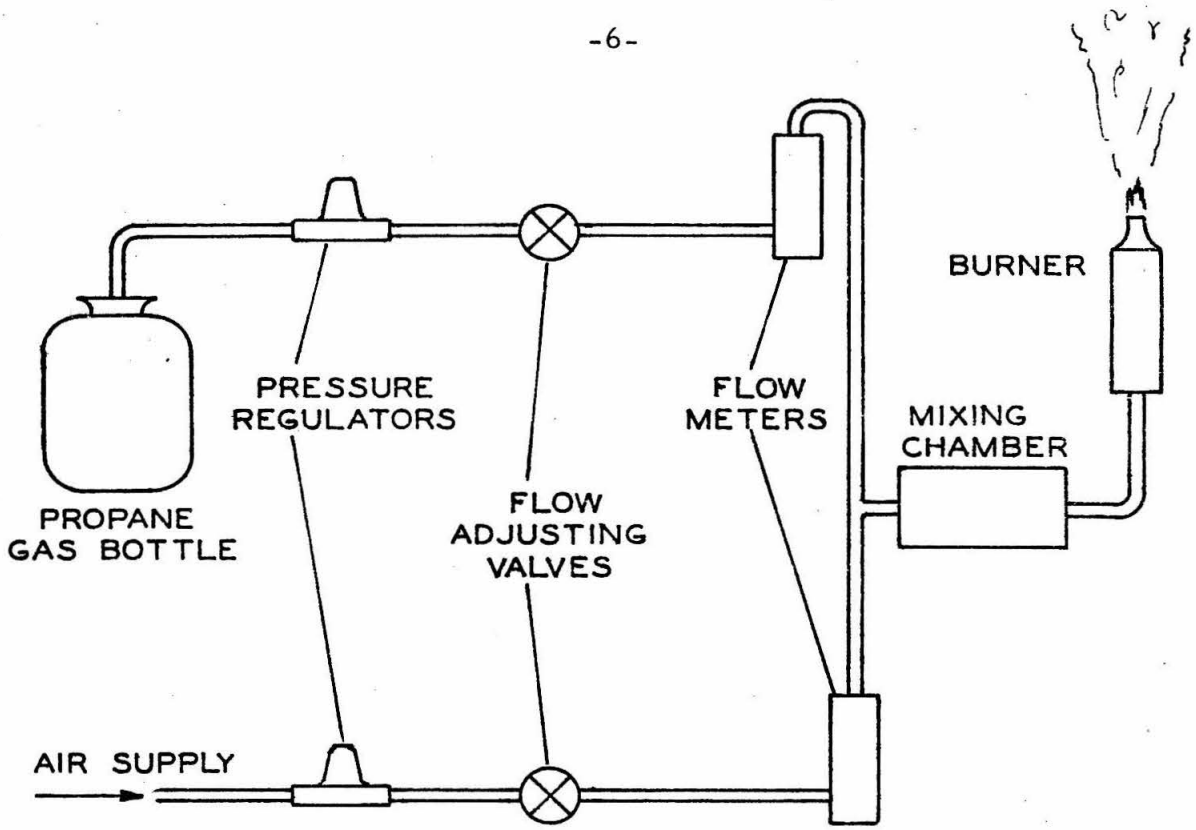

rate of fuel, the velocity at the burner exit was reduced to a value just slightly above the flame velocity of propane in order to prevent flashback into the burner. Gaydon and Wolfhard[3] estimate the stoichiometric flame velocity of propane at ~ 45 cm/sec, whereas Morgan and Kane[4], in the 4th Symposium (International) on Combustion, estimate it at approximately 41.5 cm/sec.

Using these values, calculations suggested that a 2.54 cm (1") diameter burner would yield the desired heat input and exit velocity. To further ensure stabilization of the flame and to prevent any flashback, a stainless steel grid was laid over the nozzle exit, resulting in a very stable blue flame of approximately 1/4" height.

C. Buoyant Plume

1. Scaling of the Buoyant Plume. The buoyant plume generated by a heat source was investigated by several researchers, e.g. Morton, Taylor and Turner[5], Rouse, et al.[6], Yokoi[2], and others.

Measurements conducted by the above mentioned researchers for the axisymmetric case confirmed the existence of Gaussian profiles for the mean velocity and density (or temperature) at arbitrary heights above the source:

$$\frac{u}{u_{max}} = \exp\left(\frac{-r^2}{b'^2}\right) \tag{2.1}$$

$$\frac{\Delta\rho}{\Delta\rho_{max}} = \exp\left(\frac{-r^2}{\beta^2 b'^2}\right) \tag{2.2}$$

where b' is the Gaussian width parameter based on the velocity profile. Rouse, et al.[6] measured β^2 to be 1.35.

In his investigation of finite diameter alcohol pan fires, Yokoi[2] established the fact that for heights "sufficiently far" removed from the heat source, the plume behaves independent of the source. For the purpose of this investigation, the transition from a buoyant jet to a buoyant plume needs to be considered (see the next section).

The scaling of the plume in this region of independent behavior was considered by Yokoi, and is discussed here, using a different approach yielding the same results.

Let Q' be a representative measure of the flux of heat "contained" in the buoyant plume at some arbitrary height above the source. Then

$$Q' \propto \rho V A C_p \Delta T \quad \text{(Watts)} \tag{2.3}$$

where

ρ = characteristic density

= ρ_∞ (ambient density) (kg/m^3)

V = characteristic velocity (m/s)

A = characteristic cross-sectional area of plume (m^2)

The only driving potential for the velocity is the static pressure gradient due to buoyancy:

$$\therefore V^2 \propto \frac{\Delta p}{\rho_\infty} \quad . \tag{2.4}$$

But

$$\Delta p \propto g \frac{\partial \rho}{\partial T} \Delta T \cdot z \ , \tag{2.5}$$

where z = height above the heat source (m).

$$\therefore \frac{\Delta p}{\rho_\infty} \propto gz\left(\frac{1}{\rho}\frac{\partial \rho}{\partial T}\right)\Delta T = gz\beta\Delta T \ , \tag{2.6}$$

where β = coefficient of expansion. But, assuming an ideal gas:

$$\beta = 1/T$$

$$\therefore \frac{\Delta p}{\rho_\infty} \propto gz\frac{\Delta T}{T} \ , \tag{2.7}$$

where

T = characteristic temperature

= T_∞ (ambient temperature).

Hence,

$$V^2 \propto gz\frac{\Delta T}{T_\infty}$$

$$\therefore V \propto \left(gz\frac{\Delta T}{T_\infty}\right)^{\frac{1}{2}} \quad . \tag{2.8}$$

Therefore,

$$Q' \propto \rho_\infty \left(gz \frac{\Delta T}{T_\infty} \right)^{\frac{1}{2}} A C_{p_\infty} \Delta T \quad . \tag{2.9}$$

The area A is proportional to the square of the height z for a straight-edged plume, and therefore

$$Q' \propto \rho_\infty g^{1/2} z^{5/2} \Delta T^{3/2} C_{p_\infty} \frac{1}{T_\infty^{1/2}} \quad . \tag{2.10}$$

This characteristic "heat input" can now be normalized by the heat source strength Q to form a dimensionless group:

$$\pi_1 = Q'/Q = \rho_\infty \Delta T^{3/2} g^{1/2} z^{5/2} C_{p_\infty} \frac{1}{T_\infty^{1/2} Q} \tag{2.11}$$

or

$$\pi_1' = (Q'/Q)^{2/3} = \left(\frac{g\Delta T}{T_\infty} \right) \Bigg/ z^{-5/3} \left(\frac{Qg}{\rho_\infty C_p T_\infty} \right)^{2/3} \quad . \tag{2.12}$$

This equation can be put in a more recognizable form as follows:

$$\frac{g\Delta T}{T_\infty} \Bigg/ z^{-5/3} \left(\frac{Qg}{\rho_\infty C_p T_\infty} \right)^{2/3} = \frac{\Delta T / T_\infty}{(Q^*)^{2/3}} \quad , \tag{2.13}$$

where

$$Q^* = \frac{Q}{\rho_\infty C_p T_\infty \sqrt{gz}\, z^2} \quad , \tag{2.14}$$

which clearly represents a dimensionless heat addition quantity.

Therefore, the following relationship between the maximum plume temperature and the parameters governing the problem can be expected:

$$\frac{\Delta T_{max}}{T_\infty} = C_1 (Q^*)^{2/3} \quad . \tag{2.15}$$

On page 39 of ref. 2, Yokoi arrives at a similar but slightly different equation, which can easily be shown to be equal to (2.15):

$$\Delta T_{max} = 0.423\left(\frac{T_\infty Q^2}{C_p^2 \rho_\infty^2 g}\right)^{1/3} c^{-8/9} z^{-5/3} \qquad \text{(1.112-Yokoi)}$$

$$\therefore \frac{\Delta T_{max}}{T_\infty} = 0.423\, c^{-8/9} (Q^*)^{2/3} , \qquad (2.16)$$

where, according to Yokoi,

$$c^{2/3} = 0.1 . \qquad (2.17)$$

This yields $C_1 = 9.11$ in eqn. (2.15). The results of this investigation are compared with those of Yokoi in Section IV.A.2.

A similar expression for the mean velocity on the centerline of the plume can now be derived from eqn. (2.8):

$$\frac{V}{\sqrt{gz}} = C_2 (Q^*)^{1/3} . \qquad (2.18)$$

According to Yokoi[2], C_2 is about 3.87.

Since a straight-edged plume was assumed for the above analysis, the spreading of the plume will be characterized by

$$b/z = C_3 , \qquad (2.19)$$

where b = Gaussian width parameter (based on temperature profile).

The plume spread observed during this investigation is presented and also compared with results by Alpert[1] in Section IV.A.3.

2. Transition from Buoyant Jet to Buoyant Plume. Since this investigation was concerned with the heat transfer from a buoyant plume to a ceiling, it was necessary to confirm that the physically realized plume did in fact represent a buoyant plume. The heat source used during the course of this investigation (as discussed in Section II.B above), however, represented a buoyant jet in the region close to the source, since it contained an initial momentum flux.

This momentum flux was kept as low as possible by using the lowest possible burner exit velocity which was still high enough to prevent flashback.

It was therefore necessary to investigate the transition from a buoyant jet to a buoyant plume in order to estimate the height above the source where this transition was completed, and beyond which pure plume behavior was exhibited. List and Imberger[7] investigated this transition during their study of turbulent entrainment in buoyant jets.

The characteristic quantities which determine the behavior of a buoyant jet (for the axisymmetric case) at elevation z are:

volume flux $$\dot{\mu} = \int_0^\infty 2\pi r u dr \quad (L^3T^{-1})$$

kinematic buoyancy flux $$\dot{\beta} = -\int_0^\infty 2\pi r g u \theta dr \quad (L^4T^{-3})$$

kinematic momentum flux $$m = \int_0^\infty 2\pi r u^2 dr \quad (L^4T^{-2})$$

where $u = u(r, z)$ = time-averaged axial velocity ,

$$\theta = \frac{\rho - \rho_\infty}{\rho_\infty}$$ = anomaly caused by the buoyant jet (density ρ) in the mean density field ρ_∞ .

Now, according to List and Imberger[7], the characteristic height z_o above the source with initial volume, buoyancy and momentum fluxes, $\dot{Q}$, B, and M respectively, at which the transition to a buoyant plume is completed, is given by

$$z_o = \frac{M^{3/4}}{B^{1/2}} \quad , \qquad (2.20)$$

where

$$M = \frac{\pi}{4} D^2 \overline{u}_o^{\,2} \quad ,$$

$$B = \frac{\pi}{4} D^2 g \overline{u}_o \frac{\overline{\Delta\rho_\infty}}{\rho_\infty} \quad ,$$

$$D = \text{source diameter} \quad .$$

The relation (2.20) is derived as follows. Consider the volume flux $\dot{\mu}$:

for a pure jet (i.e., no buoyancy), $\dot{\mu} \sim f_1(M, z)$

for a purely buoyant plume (i.e., no momentum) $\dot{\mu} \sim f_2(B, z)$

Hence, for a buoyant jet (i.e., initial momentum and buoyancy flux),

$$\dot{\mu} \sim f_3(B, M, z) \quad . \tag{2.21}$$

Now $\dot{\mu}$ can be put into dimensionless form as follows:

$$\overline{\mu} = \frac{\dot{\mu} B^{1/2}}{M^{5/4}} = f\left[\frac{B^{1/2} z}{M^{3/4}}\right] = f(\overline{z}) \quad .$$

Hence, for a pure jet ($B \to 0$),

$$\frac{B^{1/2} z}{M^{3/4}} << 1 \quad .$$

Therefore, a linear approximation (first order) for the function f yields

$$\overline{\mu} \sim \overline{z} \quad . \tag{2.22}$$

On the other hand, for a purely buoyant plume ($M \to 0$),

$$\frac{z B^{1/2}}{M^{3/4}} >> 1 \quad .$$

M can then be eliminated by letting

$$\frac{\dot{\mu} B^{1/2}}{M^{5/4}} \sim \left[\frac{B^{1/2} z}{M^{3/4}}\right]^{5/3} \quad ,$$

or

$$\bar{\mu} \sim \bar{z}^{5/3} \quad . \tag{2.23}$$

Based on experimental results obtained by List and Imberger[7], it can be concluded that the transition to a buoyant plume is completed when

$$\bar{z} = 1$$

or

$$z_o = \frac{M^{3/4}}{B^{1/2}} \quad . \tag{2.20}$$

Hence, to estimate this value of z_o, the following values obtained from Eckert and Drake[8] were used:

$$\overline{\Delta\rho_\infty} = \rho_\infty - \bar{\rho}_{ne}$$

ρ_∞ = ambient density $\simeq \rho_{\substack{air \\ 300^oK}} = 1.18 \text{ kg/m}^3$

$\bar{\rho}_{ne}$ = average density of combustion products at nozzle exit immediately after combustion

$\simeq \rho_{\substack{air \\ 2000^oK}} = 0.18 \text{ kg/m}^3$

For source strength $Q = 1.17$ kW,

$$\bar{u}_o \simeq 0.7 \text{ m/s} \qquad \text{(see Appendix A)} \quad ,$$

$$D = 1'' = 2.54 \times 10^{-2} \text{ m} \quad .$$

This yields

$$B = 29.5 \times 10^{-4} \text{ m}^4/\text{s}^3 \quad ,$$

$$M = 2.48 \times 10^{-4} \text{ m}^4/\text{s}^3 \quad .$$

$$\therefore \quad z_o = 0.036 \text{ m} = 3.6 \text{ cm} \qquad (\simeq 1.4'') \quad .$$

In the case of a heat source strength $Q = 1.53$ kW (utilizing the same burner),

$$\bar{u}_o \simeq 1.07 \text{ m/s} \quad .$$

$$\therefore \quad z_o = 0.055 \text{ m} = 5.5 \text{ cm} \qquad (\simeq 2.2") \ .$$

From these estimates it can therefore be concluded that at elevations an order of magnitude larger than z_o (i.e., for $z > 0.36$ m), the plume is fully buoyant. Plume measurements in this region agreed very well with experimental data for purely buoyant plumes obtained by Yokoi[2] (see Section IV. A).

3. Plume Temperatures. Temperature measurements at various positions throughout the plume were required in order to define and characterize the buoyant plume resulting from the heat source used during these experiments. These measurements were not carried out with the intention of investigating the entrainment phenomena associated with such a plume, but merely to enable the author to characterize this specific plume and compare the results with those obtained by other investigators.

a) Radial temperature measurements. These temperature measurements were conducted with the purpose of obtaining a measure of i) the radial growth of the plume as a function of the height z above the heat source; and ii) agreement of the typical radial temperature variation with the theoretical model in which a Gaussian distribution of the following form is assumed:

$$\Delta T / \Delta T_{max} = \exp(-r^2/b^2)$$

where $\Delta T = T - T_\infty$,

$$\Delta T_{max} = T_{max} - T_\infty$$

T_∞ = ambient temperature

b = Gaussian width parameter based on the temperature profile

i.e., $r = b$, where $\Delta T = \frac{1}{e} \Delta T_{max}$.

b) Centerline temperature measurements. The centerline (or maximum plume) temperatures were obtained by traversing horizontally across the plume at different heights. This enabled the author to compare his data with those obtained by other researchers using similar and different heat sources. In particular, these data are compared with those obtained by Yokoi[2] during experiments with point and finite diameter heat sources (alcohol fires), and correlated with the scaling laws developed during the course of his experiments. The results are presented in Section IV. A.

D. Ceiling Jet

A ceiling jet (or more generally termed, a wall jet) develops when a jet of fluid impinges normally on a flat surface. The resulting jet can either be an axisymmetric wall jet, in which the flow along the surface is radially outward, or a two-dimensional jet. The flow in such a jet can either be laminar or turbulent, depending on the condition of the impinging jet; but in most practical cases the wall jet will be turbulent.

The wall jet has been the subject of various theoretical and experimental investigations. Glauert[9] treats the isothermal wall jet from a theoretical point of view, applying similarity solutions to the boundary layer equations to find similarity exponents for the maximum velocity variation and jet growth (width) as a function of distance. Bakke[10] conducted an experimental investigation of a turbulent,low-speed wall jet on a smooth, flat plate and correlated

his results with the theoretical solutions proposed by Glauert.

The experimental investigation reported in this paper was concerned with the heat transfer from a ceiling jet, developing as the result of a buoyant plume of hot gas rising from a heat source (fire) and impinging on a horizontal, unobstructed ceiling. Clearly, this situation is related to that of a low-speed turbulent jet impinging on a flat plate, the only difference being the fact that the ceiling jet contains an excess temperature which decreases with radial distance due to heat transfer to the ceiling and to entrainment of cooler ambient air. Such a hot ceiling jet was the subject of the investigation by Alpert[1], the results of which are compared with those obtained during this experiment.

Again, it needs to be emphasized that the aim of the experimental investigation reported here was to conduct measurements of the heat transferred from the ceiling jet to the ceiling, without attempting to analyze in detail the flow in the ceiling jet and the accompanying entrainment phenomena as reported by Alpert.

1. Vertical Temperature Distribution. The vertical temperature variation in the ceiling jet (from the ceiling downward) at various radial positions was obtained with the purpose of i) finding the general temperature profile in order to compare the agreement with the theoretical model of a Gaussian temperature distribution given by

$$\Delta T/\Delta T_{max} = \exp(-y^2/\ell^2) ,$$

ℓ = Gaussian width parameter based on temperature profile (i.e., $y = \ell$ where $\Delta T = \frac{1}{e}\Delta T_{max}$); ii) to find a scaling parameter for the variation of the maximum ceiling jet temperature as a function of the

outward radius (see Section 2. below).

2. Non-dimensionalizing Ceiling Jet Maximum Temperature. From the point of view of heat transfer prediction, the maximum temperature in the ceiling jet (given as a function of the outward radius) is the most appropriate variable for characterizing the ceiling jet and relating it to the buoyant plume and hence to the heat source. The following analysis yields appropriate parameters for non-dimensionalizing this maximum temperature and also relating it to the strength of the heat source Q and the ceiling height H above the source.

It can be assumed that the ceiling jet maximum temperature at the exit plane of the turning region is proportional to the plume maximum temperature at the corresponding height, i.e.,

$$\Delta T_{\substack{\max \\ \text{ceiling jet}}} \propto \Delta T_{\substack{\max \\ \text{plume}}} \tag{2.24}$$

Hence, from eqn. (2.15), letting z = H (ceiling height), a relationship between the maximum ceiling jet temperature at the exit plane and the governing flow parameters is obtained:

$$\frac{\Delta T_{\max}}{T_\infty} = C_4 (Q^*)^{2/3} \tag{2.25}$$

where now

$$Q^* = \frac{Q}{\rho_\infty C_p T_\infty \sqrt{gH}\, H^2} \quad , \tag{2.26}$$

H = ceiling height .

This yields the dimensionless group:

$$\pi_1 = \frac{\Delta T / T_\infty}{(Q^*)^{2/3}} \quad . \tag{2.27}$$

To determine the variation of the maximum ceiling jet temperature with radius, a second dimensionless group involving the geometry of the problem can be formed, by dividing the radius along the ceiling by the ceiling height,

$$\pi_2 = r/H \quad . \tag{2.28}$$

From (2.27) and (2.28), the following functional relationship between the dimensionless ceiling jet temperature and the dimensionless radial position can be expected:

$$\frac{\Delta T_{max} / T_\infty}{(Q^*)^{2/3}} = f_1(r/H) \quad . \tag{2.29}$$

This is the same relationship derived by Alpert[1] during a theoretical analysis of the ceiling jet.

The agreement of experimental data with eqn. (2.29) is discussed in Section IV. B.

E. Heat Transfer Model

The model used for doing ceiling heat transfer measurements was determined by the technique employed for measuring such heat transfer. The basic requirements for such a heat transfer model were:

i) the heat transfer measured locally had to be representative of the heat transfer at all other positions with the same radius (i. e., for the axisymmetric case);

ii) no local disturbances in the ceiling jet and changes in the thermal properties, surface roughness, etc. of the ceil-

ing had to be induced;

iii) measurements at several different radial positions had to be done at the same time.

Several methods of heat transfer measurements were considered. A study of the use of heat flux gauges (commercially available) was made, and revealed that the properties of such devices, e.g. conductivity, thickness, size, surface roughness, etc., might cause a substantial error in the heat flux measured locally; e.g. the conductivity of a typical heat flux gauge is of the order of 0.36 $W/m\,^{o}K$ ($\simeq$ 2.5 $Btu\text{-}in/ft^2\text{-}hr$). Unless this gauge is used on a ceiling with conductivity of the same order of magnitude, the gauge might act locally as a heat barrier (or conversely). An additional disadvantage of such heat flux gauges is their cost; and since it was required to do heat transfer measurements at different radial positions simultaneously, the use of several such devices could become costly.

The above considerations and limitations suggested use of the transient method for measuring ceiling heat transfer. This method consisted basically of measuring the ceiling temperature periodically over the required time interval, and using the derivative of the temperature with respect to time to calculate the increase in the ceiling internal energy (locally) due to heat transfer from the ceiling jet. Applying corrections for the heat losses through radial conduction and from the upper side of the ceiling, the heat transfer from the ceiling jet as a function of radius and time was obtained.

Preliminary experiments proved this method to be successful and of relatively low cost.

However, it was realized that the correction due to radial conduction might be substantial. Consider the ratio between the radial conduction of heat and the increase in internal energy of the ceiling:

$$\frac{q_{cond}}{\Delta E} \propto \frac{\delta k\left[\frac{1}{r}\frac{\partial}{\partial r}\left(r\frac{\partial T}{\partial r}\right)\right]}{\rho C\delta\left(\frac{\partial T}{\partial t}\right)} ,$$

where

δ = ceiling thickness

k = conductivity

ρ = ceiling density

C = specific heat

$$\therefore \frac{q_{cond}}{\Delta E} \propto \frac{\varkappa\left[\frac{1}{r}\frac{\partial}{\partial r}\left(\frac{\partial T}{\partial r}\right)\right]}{\partial T/\partial t} . \qquad (2.30)$$

Hence, in order to keep the radial conduction as low as possible, the thermal diffusivity of the ceiling had to be as low as possible. (Note that the ceiling thickness has no influence.)

However, for evaluating the increase in ceiling internal energy, the assumption had to be made that a uniform temperature existed throughout the ceiling. This would be the case if a) the ceiling was relatively thin; b) the conductivity of the ceiling material was large enough. Furthermore, to ensure a convenient rate of increase of the ceiling temperature, the conductivity of the ceiling material could not be too low.

Several preliminary experiments revealed that a ceiling of 1/16" cold-rolled steel plate would exhibit the desired thermal behavior for the heat source strength required during these experi-

ments. Such a ceiling had the additional advantage of simplifying the method of attachment of thermocouple junctions, since these could simply be spot-welded onto the ceiling.

Ceiling heat transfer measurements had to be carried out for ceiling heights ranging between 50 cm (≃ 20") to 82 cm (≃ 32") above the heat source. It was estimated that at these heights the buoyant plume would have a diameter of 23 cm (9") to 30 cm (12"). This suggested that a ceiling of 91 cm (36") diameter would be adequate for the purpose of ceiling heat transfer measurements, since the ratio of ceiling height to width is representative of that of a normal room.

The back of the ceiling was insulated with 9 cm ($3\frac{1}{2}$") thick glass wool insulation to reduce the heat loss from this surface. It was, however, still necessary to correct for the heat loss through this insulating material, as discussed below.

1. Determining the Ceiling Heat Transfer. Consider a typical volume element of the ceiling material:

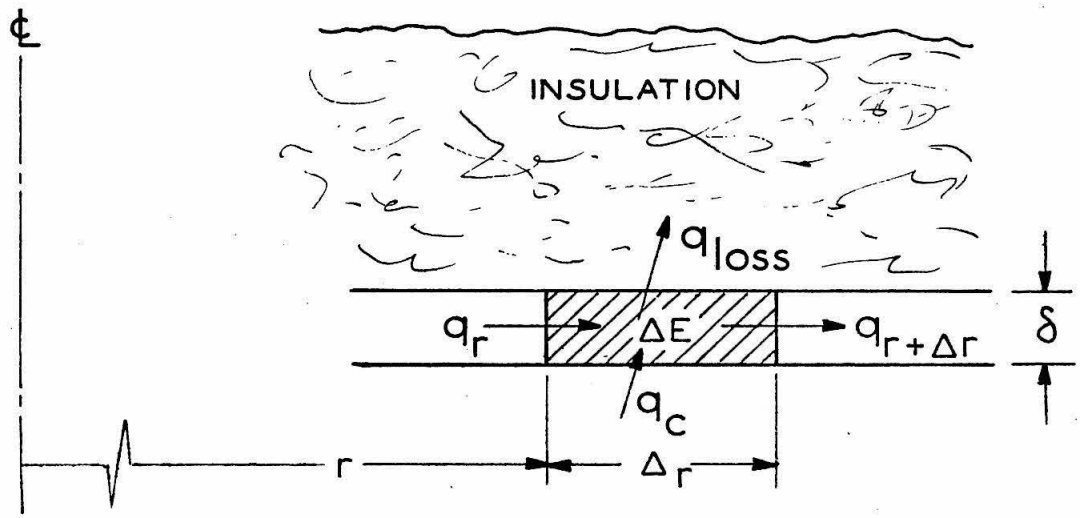

Energy balance:

$$\Delta E = q_{in} - q_{out}$$

$$= q_c - q_{loss} - (q_{r+\Delta r} - q_r) .$$

$$\therefore \quad q_c = \Delta E + q_{loss} + q_{cond} , \tag{2.31}$$

where

q_{loss} = heat loss through backing insulator/unit area

q_{cond} = radial heat conduction/unit area = $q_{r+\Delta r} - q_r$

q_c = ceiling heat transfer/unit area

a) Increase in ceiling internal energy (ΔE). The increase in ceiling internal energy was obtained by measuring the ceiling temperature periodically at seven radial positions, spaced 7 cm apart starting from the center of the ceiling. The temperature at each position was measured every 44 sec (refer to Section III. B). To confirm axisymmetry, the same measurements were carried out on two other radii 120° apart.

These measurements were carried out over a period of 9 minutes from the time the burner was started, yielding twelve temperatures as a function of time for each radial position.

Two techniques were applied for obtaining ΔE from these data. i) The data points were plotted on large-scale graph paper, a smooth curve drawn through all points, and a tangent constructed geometrically at each position at the required times. Though somewhat time consuming, this method yielded good results. ii) The second technique required the use of a computer program to do a least-squares fit of any required degree polynomial (degree of polynomial

less than number of points) to the data points. After several attempts with different values for the degree of polynomial fit and comparison with data obtained through method i), it was found that a sixth degree polynomial yielded almost exactly the same values as method i). This method helped a great deal to accelerate the reduction of the data.

The results obtained from either method i) or ii) were then substituted into the equation;

$$\Delta E(r,t) = \rho C \delta \left.\frac{\partial T}{\partial t}\right|_{r,t} \qquad (W/m^2) \ . \tag{2.32}$$

b) Radial heat conduction. Under the assumption of an axi-symmetric case (i.e., no tangential temperature gradients) and a uniform ceiling temperature (δ sufficiently small), the radial heat conduction due to a radial temperature gradient only (assuming positive radially outward) is given by:

$$q_{cond} = -\delta k \left(\frac{\partial^2 T}{\partial r^2} + \frac{1}{r} \frac{\partial T}{\partial r} \right) \qquad (W/m^2)$$

$$= -\delta k \left[\frac{1}{r} \frac{\partial}{\partial r} \left(r \frac{\partial T}{\partial r} \right) \right] \ . \tag{2.33}$$

Since the value of q_{cond} at the center was required, the singularity at $r = 0$ was removed by writing (2.33) in the following form:

$$q_{cond} = -\delta k \, 2 \frac{\partial}{\partial (r^2)} \left(2r^2 \frac{\partial T}{\partial (r^2)} \right) \ .$$

Letting $R = r^2$, this equation becomes

$$q_{cond}(r,t) = -4\delta k \frac{\partial}{\partial R} \left(R \frac{\partial T}{\partial R} \right) \Big|_{r,t} \ . \tag{2.34}$$

Evaluation of eqn. (2.34) therefore required the calculation of $\partial T/\partial R$ and $\frac{\partial}{\partial R} \left(\frac{\partial T}{\partial R} \right)$.

T(R) at any required time was obtained from the temperature history for the seven radial positions. Then $\partial T/\partial R$ was evaluated graphically, multiplied by the value of R corresponding to each position, and the slope $\frac{\partial}{\partial R}\left(\frac{\partial T}{\partial R}\right)$ determined graphically.

Such graphical procedures, especially in evaluating the second derivative, introduce a large degree of inaccuracy, and the author admits that this constitutes a limitation on the accuracy of these results.

In evaluating the second derivative, it was found that at positions r = 0 and r = 7 cm, the slopes of the curves became so large that graphical evaluation became impossible. It was therefore decided to use the data for the first four radial positions for fitting a theoretical curve through these points, using the computer program mentioned above. This enabled calculation of the second derivative with greater accuracy than is graphically possible.

The procedure followed was:

<u>at r = 0</u>

Consider a Taylor expansion of $T(r^2)$ at r = 0 .

$$T = T_o + \left(\frac{\partial T}{\partial R}\right)_0 R + (\quad)R^2 + \ldots$$

$$\therefore \frac{\partial T}{\partial R} = \left(\frac{\partial T}{\partial R}\right)_0 + 2R(\quad) + \ldots$$

$$R\frac{\partial T}{\partial R} = R\left(\frac{\partial T}{\partial R}\right)_0 + 2R^2(\quad) + \ldots$$

$$\therefore \frac{\partial}{\partial R}\left(R\frac{\partial T}{\partial R}\right) = \left(\frac{\partial T}{\partial R}\right)_0 + 4R(\quad) + \ldots$$

Hence, at $R = r^2 = 0$:

$$\frac{\partial}{\partial R}\left(R\,\frac{\partial T}{\partial R}\right)\Big|_0 = \left(\frac{\partial T}{\partial R}\right)_0 \quad . \tag{2.35}$$

Now let $T(r^2)$ be represented by the following third degree polynomial:

$$T = a_o + a_1 r^2 + a_2 (r^2)^2 + a_3 (r^2)^3 = a_o + a_1 R + a_2 R^2 + a_3 R^3 \quad .$$

then

$$\frac{\partial T}{\partial R} = a_1 + 2a_2 R + 3a_3 R^2 \quad . \tag{2.36}$$

Hence, from eqn. (2.35),

$$\frac{\partial}{\partial (r^2)}\left[r^2 \left(\frac{\partial T}{\partial (r^2)} \right) \right]_0 = \frac{\partial T}{\partial R}\Big|_0 = a_1 \tag{2.37}$$

$$\therefore \quad q_{cond}(0,t) = -4\delta k a_1 \quad . \tag{2.38}$$

<u>at $r = r_1$</u>

From (2.36):

$$R\,\frac{\partial T}{\partial R} = a_1 R + 2a_2 R^2 + 3a_3 R^3 \quad .$$

$$\therefore \quad \frac{\partial}{\partial R}\left(R\,\frac{\partial T}{\partial R}\right) = a_1 + 4a_2 R + 9a_3 R^2 \quad . \tag{2.39}$$

Hence, radial conduction at $r = r_1$ is given by:

$$q_{cond}(r_1, t) = -4\delta k[a_1 + 4a_2 R + 9a_3 R^2] \quad . \tag{2.40}$$

This method could not be extended to the remaining five radial positions, since the multiplication by r^2 before taking the second derivative tended to make the function very sensitive to any error in the polynomial fit for the first derivative. This was proved by applying the technique to one set of data points. Hence, the graphical method was used to evaluate q_{cond} at the remaining five positions. It was also proved by the first experiment that the contribution of the radial conduction term at these remaining five positions was at least

an order of magnitude smaller than that of the increase in internal energy. An error in these estimates, therefore, could not contribute a significant error in the overall heat transfer.

c) Heat loss through the backing insulator. Though glass-wool insulation was used on the upper surface of the ceiling to reduce heat loss from this surface, the absence of perfect insulation required the calculation of the heat conducted through this insulator. Assuming that the insulation is in good thermal contact with the upper surface of the ceiling, the temperature of the contact surface of the insulation will assume that of the ceiling, and vary accordingly. Then the insulator can be considered to be a semi-infinite solid, with a known temperature variation on the surface. An approximation (of second order) is made by ignoring the radial conduction through the insulator due to a radial temperature gradient at the surface. Under these assumptions, the following analysis can be made.

Consider the one-dimensional heat conduction equation:

$$\frac{\partial T}{\partial t} = \varkappa \frac{\partial^2 T}{\partial x^2} \quad , \qquad x > 0 \qquad (2.41)$$

$$T = 0 \text{ at } t = 0$$

$$T = T_c(t) \text{ at } x = 0$$

where T_c = ceiling temperature. Applying the Laplace Transform:

$$\overline{T} = \int_0^\infty T e^{-st}\, dt \ .$$

Then (2.41) becomes

$$\frac{\partial^2 \overline{T}}{\partial x^2} - \frac{s}{\varkappa} \overline{T} = 0 \ .$$

Solving this differential equation gives

$$\overline{T} = \overline{T}_c(s)\, e^{-x\sqrt{s/\kappa}} \quad .$$

$$\therefore \quad \frac{\partial \overline{T}}{\partial x}\Big|_{x=0} = -\frac{s}{\sqrt{\kappa}}\,\frac{1}{\sqrt{s}}\,\overline{T}_c(s) \quad .$$

Now appling the inverse transform:

$$\frac{\partial T}{\partial x}\Big|_{x=0} = -\frac{1}{\sqrt{\pi\kappa}}\,\frac{d}{dt}\int_0^t \frac{T_c(\tau)}{\sqrt{t-\tau}}\,d\tau = \frac{1}{\sqrt{\pi\kappa}}\int_0^t \frac{T'_w(\tau)}{\sqrt{t-\tau}}\,d\tau \quad \text{if} \quad T_w(0) = 0 \quad .$$

$$\therefore \quad q_{loss} = \sqrt{\frac{1}{\pi}(\rho Ck)_{ins}}\int_0^t \frac{T'_w(\tau)}{\sqrt{t-\tau}}\,d\tau \quad . \tag{2.42}$$

Now let

$$T'_w(t) = a_o + a_1 t + a_2 t^2 + \ldots = \sum_{n=0}^{\infty} a_n t^n \quad .$$

Then

$$q_{loss}\sqrt{\frac{\pi}{(\rho Ck)_{ins}}} = \sum_{n=0}^{\infty} a_n \int_0^t \frac{\tau^n}{\sqrt{t-\tau}}\,d\tau = \sum_{n=0}^{\infty} a_n t^{n+\frac{1}{2}} \int_0^1 \frac{z^n}{\sqrt{1-z}}\,dz \quad , \tag{2.43}$$

where $\tau = tz$.

$$\int_0^1 \frac{z^n}{\sqrt{1-z}}\,dz = B(n+1,\ 1/2)$$

$$= \frac{\Gamma(n+1)\Gamma(1/2)}{\Gamma(n+3/2)}$$

$$= \frac{2.2^{2n}(n!)^2}{(2n+1)!} = 2c_n$$

$$c_o = \frac{2^o(O!)^2}{2!} = 1 \tag{2.44}$$

$$\frac{c_n}{c_{n-1}} = \frac{2^{2n}(n!)^2}{(2n+1)!}\,\frac{(2n-1)!}{2^{2n-2}(n-1)!} = \frac{2^2 n^2}{(2n+1)2n} = \frac{2n}{2n+1} \quad .$$

$$\therefore \quad c_n = \frac{2n}{2n+1} c_{n-1} \quad ; \qquad n \geq 1 \tag{2.45}$$

Hence,

$$q_{loss}(r,t) = \frac{2}{\sqrt{\pi}} [(\rho ck)_{ins} t]^{\frac{1}{2}} \sum_{n=0}^{\infty} a_n c_n t^n \quad . \tag{2.46}$$

The values of ρ and k for the insulation used in this experiment were obtained from the manufacturer's research laboratories. The value for the specific heat (C) was not available, but with the values of ρ and k known for the insulator, air, and glass wool, C was calculated (see Appendix B).

2. Ceiling Heat Transfer Coefficient. Substituting for the values of ΔE, q_{cond}, and q_{loss} in eqn. (2.31), the total amount of heat transferred per unit area of the ceiling can be calculated as a function of the radial position and time. From this it is possible to define a ceiling heat transfer coefficient:

$$h_c(r,t) = \frac{\Delta T}{q_c} \qquad (W/m^2\ ^oK) \tag{2.47}$$

where

$\Delta T = T_g - T_c$,

T_c = ceiling temperature ,

T_g = some reference temperature in the ceiling jet.

The problem in defining such a heat transfer coefficient is the choice of the appropriate reference temperature (T_g) in the ceiling jet. Basically, there exist three possible reference temperatures:

i) an average ceiling jet temperature at time t and position r,

ii) the maximum ceiling jet temperature at t and r ,

iii) the maximum temperature the ceiling jet would reach in the case of an adiabatic wall (i.e., the recovery temperature),

measured adjacent to the wall at r .

The choice of any of these temperatures presented some problems. The average ceiling jet temperature is not directly measurable and can only be calculated if the temperature profile through the ceiling jet at every radial position is known. On the other hand, the maximum ceiling jet temperature can be measured, but the distance below the ceiling where this temperature occurs is not easily defined and may vary with time. Since the adiabatic wall temperature was easier to measure and could also be calculated most easily, it seemed to be the most appropriate reference temperature.

It is debatable whether an "adiabatic wall" condition is in fact reached, even after a long time. Preliminary experiments indeed revealed that,due to a large radial conduction component near the center of the plate, some heat transfer still occurred even after a very long time, resulting in a noticeable difference between the gas and ceiling temperatures. However, this occurred mainly in the turning region where the hot gas flowed from the buoyant plume to the ceiling jet (also called the stagnation region). For radial positions farther out, the ceiling did reach the gas temperature so that an "adiabatic wall" condition was established, with the maximum temperature measured adjacent to the wall.

Based on these considerations, the ceiling heat transfer coefficient was defined as

$$h_c(r,t) = \frac{T_{ad} - T_c}{q_c} \qquad (W/m^2) \qquad (2.48)$$

where $T_{ad} \equiv$ "adiabatic wall" temperature which is measured after

$\simeq$ 30 minutes in the work discussed here.

This heat transfer coefficient can be put into a much more useful form, by relating it to the other parameters which characterize this problem.

3. Dimensionless Ceiling Heat Transfer Coefficient. Consider the Stanton number defined as

$$St = \frac{h_c}{\rho_g V_g C_p} \quad , \tag{2.49}$$

where

V_g = characteristic velocity in ceiling jet,

ρ_g = characteristic gas density,

C_p = specific heat of gas.

In analogy to the non-dimensionalizing of the ceiling jet maximum temperature, let

$\rho_g = \rho_\infty$ = ambient density,

$C_p = C_{p_\infty}$ = ambient specific heat.

Now it is reasonable to assume that the ceiling jet velocity is proportional to the velocity in the buoyant plume as a result of buoyancy only. Hence, from (2.8),

$$\therefore \quad V_g \propto (gH\,\Delta T/T_\infty)^{1/2}$$

$$\therefore \quad St \propto \frac{h_c T_\infty^{1/2}}{\rho_\infty C_p g^{1/2} H^{1/2} \Delta T^{1/2}} \quad . \tag{2.50}$$

Since ΔT in the ceiling jet is related to the maximum plume temperature, let

$$\Delta T \propto \Delta T_{ad} = (T_{ad} - T_\infty) \quad .$$

Then, from (2.29),

$$\Delta T^{1/2} \propto \frac{T_\infty^{1/2}}{g^{1/2}} H^{-5/6}\left(\frac{Qg}{\rho_\infty C_p T_\infty}\right)^{1/3}\left[f_1\left(\frac{r}{H}\right)\right]^{1/2} .$$

Hence,

$$St \propto \frac{h_c}{\rho_\infty C_p} \frac{H^{1/3}}{(Qg/\rho_\infty C_p T_\infty)^{1/3}}\left[f_1\left(\frac{r}{H}\right)\right]^{-1/2} . \qquad (2.51)$$

Therefore, the following relationship can be expected:

$$\frac{h_c}{\rho_\infty C_p (Qg/\rho_\infty C_p T_\infty H)^{1/3}} = f_2\left(\frac{r}{H}\right) . \qquad (2.52)$$

This is the same dimensionless parameter derived by Alpert[1] in his analysis of the ceiling heat transfer.

Following the treatment of the dimensionless ceiling jet temperature (see the previous section), eqn. (2.52) can be put into an easier recognizable and simpler form as follows:

$$\frac{h_c}{\rho_\infty C_p (Qg/\rho_\infty C_p T_\infty H)^{1/3}} = \frac{h_c}{\rho_\infty C_p \sqrt{gH}\,(Q^*)^{1/3}} ,$$

where, as before,

$$Q^* = \frac{Q}{\rho_\infty C_p T_\infty \sqrt{gH}\, H^2} .$$

Hence,

$$\frac{h_c}{\rho_\infty C_p \sqrt{gH}\,(Q^*)^{1/3}} = f_2\left(\frac{r}{H}\right) \equiv h_c' . \qquad (2.53)$$

A very interesting and simple relationship between q_c, Q, and H is obtained for the case where $T_c = T_\infty$, i.e., at the beginning of the experiment when the ceiling temperature is equal to the ambient temperature. By multiplying the dimensionless group π_1 [eqn. (2.27)] and the Stanton number as defined by eqn. (2.51), the

following result is obtained:

$$\pi_3 = \frac{g\Delta T_{ad}}{T_\infty} \frac{H^{1/3}}{H^{-5/3}\left(\frac{Qg}{\rho_\infty C_p T_\infty}\right)\rho_\infty C_p} = \frac{h_c \Delta T_{ad} H^2}{Q} \quad . \quad (2.54)$$

Now, if $T_c = T_\infty$, then the initial ceiling heat transfer rate is

$$\dot{q}_c^* = h_c(T_g - T_\infty) = h_c \Delta T_{ad} \quad .$$

Hence, (2.54) becomes

$$\pi_3 = \frac{\dot{q}_c^* H^2}{Q} \quad . \quad (2.55)$$

Therefore, it can be expected that when a fire starts out, the following relationship will hold:

$$\frac{\dot{q}_c^* H^2}{Q} = f_3\left(\frac{r}{H}\right) \quad . \quad (2.56)$$

Thus, in the early stages of a fire, the ceiling heat transfer will vary as Q/H^2 .

4. Time Scale for Heat Transfer Model. Since the buoyant plume is of a steady nature, the time scale for the ceiling temperature depends only on the ceiling. This time scale, assuming a thin slab ceiling and ignoring radial conduction as well as losses from the upper side of the ceiling, can be derived as follows.

Consider an element of the ceiling to which heat $\dot{q}_c$ per unit area is transferred. Under the above assumptions the energy equation yields

$$\rho_c C_c \delta \frac{\partial T}{\partial t} = \dot{q}_c = h_c(T_{ad} - T) \quad ,$$

which can be written as

$$\left(\frac{1}{T_{ad}-T}\right)\frac{\partial(T_{ad}-T)}{\partial t} = -\frac{h_c}{\rho_c C_c \delta} \quad . \tag{2.57}$$

Preliminary experiments showed h_c to be reasonably constant during the first 8 - 10 minutes.

Thus, eqn. (2.57) can be integrated to give

$$\frac{T_{ad} - T}{T_{ad} - T_o} = e^{-\tau} \quad , \tag{2.58}$$

where

$$\tau = \frac{h_c}{\rho_c C_c \delta} \quad ,$$

and $T_o \equiv T_\infty \equiv$ initial ceiling temperature.

Substituting for h_c from eqn. (2.53) yields

$$\tau = \left(\frac{\rho_\infty C_{p_\infty}}{\rho_c C_c}\right)\frac{\sqrt{gH}\, t}{\delta}(Q^*)^{1/3} f_2\left(\frac{r}{H}\right) \quad . \tag{2.59}$$

Hence, choosing as the value for the characteristic time scale, τ_c,

$$\tau_c = 1 \quad ,$$

i.e.,

$$\frac{T_{ad}-T}{T_{ad}-T_o} = \frac{\Delta T_{ad} - (T-T_o)}{\Delta T_{ad}} = \frac{1}{e} \quad ,$$

or

$$\frac{T-T_o}{\Delta T_{ad}} = \frac{\Delta T_c}{\Delta T_{ad}} = 1 - \frac{1}{e} \tag{2.60}$$

yields the following relation for the dimensionless characteristic time:

$$\frac{t_c\sqrt{gH}}{\delta} = \left(\frac{\rho_c C_c}{\rho_\infty C_{p_\infty}}\right)(Q^*)^{-1/3}\left[f_2\left(\frac{r}{H}\right)\right]^{-1} \quad . \tag{2.61}$$

III. INSTRUMENTATION

A. Heat Source Strength

No special instrumentation was required for determining the magnitude of the heat released by the burner. As discussed in Section II. B, the gas and air flows were metered through two Fischer-Porter rotameter-type flowmeters, and controlled by two adjustable valves. The flowmeters were calibrated for gas and air flow, respectively, taking care that during calibration the exit pressure resembled that in the actual experiment as closely as possible. From the known gas and air volumetric flow rates, the heat input was calculated as described in Appendix A.

Once adjusted to the required value, these flow rates remained constant throughout each experiment, and no further adjustments were necessary during the course of the experiment.

B. Temperature Measurements

1. Plume Temperature Measurements. Thermocouples were used for measuring temperatures in the buoyant plume. To reduce errors in the measured temperatures due to radiative heat transfer and conduction along the thermocouple leads, the diameter of the wire had to be as small as possible. This was achieved by using .005" diameter iron and constantan thermocouple wires, coated with a thin teflon layer (generally known as a type J junction). The hot junction was made by spot welding the bare wires together. This ensured a good electrically-conducting junction with no added thermal capacity due to additional metal used in forming the junction. The thermocouple was then placed in a 1/8" diameter stainless-steel tube

and epoxied in position with the hot junction at least 1/4" away from the end of the tube.

The e.m.f. produced by these thermocouples is in the order of 10 mV for the temperature range expected in these experiments. In order to record these temperature measurements on a strip chart recorder, the output from the thermocouple had to be amplified. A DC amplifier with a gain of 100 was used, thus producing an output in the order of 0.1 V, which could be recorded to within the accuracy available on the recorder.

Trial plume temperature measurements confirmed the expected fluctuating nature of the temperature in the plume, due largely to the turbulent nature of the buoyant plume and the entrainment of the cooler surrounding air. These temperature fluctuations varied in magnitude, depending on the position in the plume and the height above the heat source. A closer study of these temperature fluctuations revealed the existence of very low frequency variations (approximately 0.5 cycle/min) of relatively small amplitude, and imposed on these were higher frequency fluctuations (approximately 2 - 4 cycles/sec) with large amplitudes ranging from 5 ^{o}C at the outer edge of the plume to approximately 30 - 40 ^{o}C on the centerline of the plume (decreasing with an increase in elevation above the source). Since this part of the investigation was mainly concerned with defining the plume, based on average temperatures, and also due to the fact that at these higher frequency fluctuations the thermal capacity of the thermocouple junction affects the measured temperature, a filtering circuit was built into the amplifier circuit discussed above.

It was important, however, not to filter out the lower frequency fluctuations, since it was suspected that these might be due to some large scale movement of the plume as a whole. Therefore, it was decided to use a filtering circuit that would filter out frequencies in excess of 1 cycle/sec.

A circuit diagram of the amplifier with built-in filter is shown below.

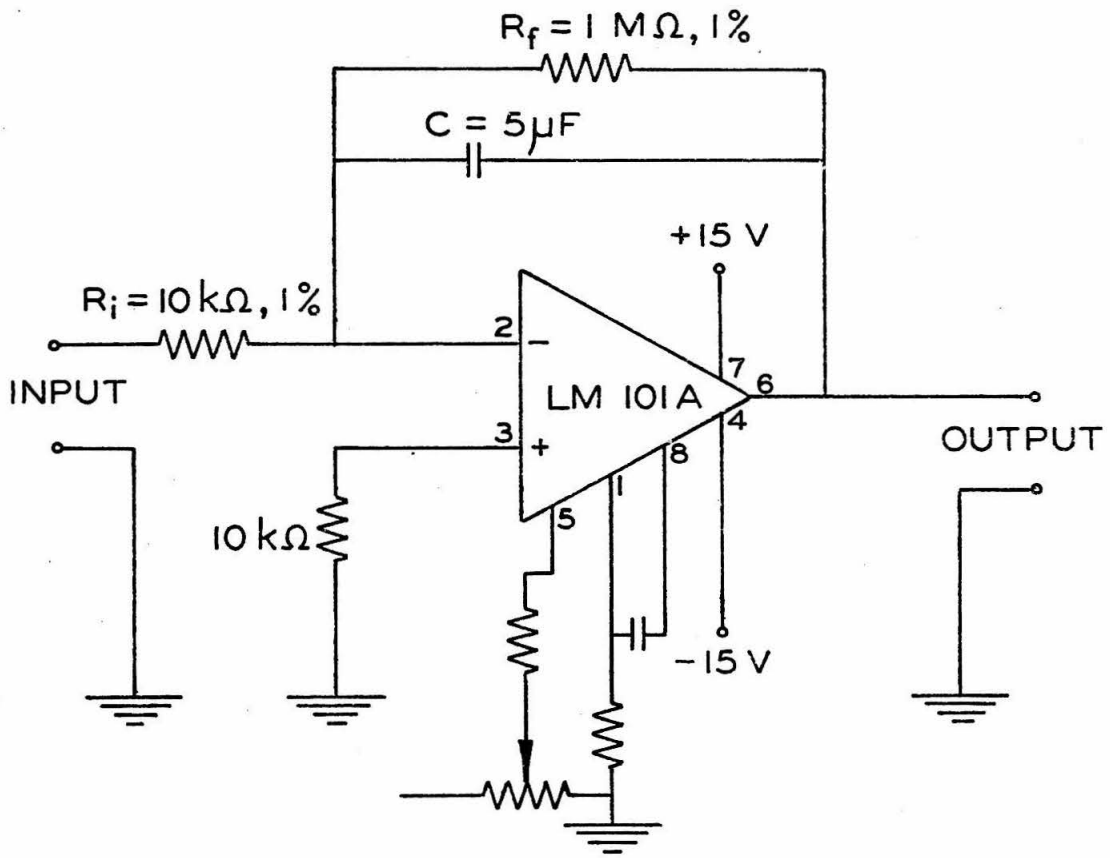

$$\text{Transfer function} = -\frac{R_f}{R_i}\,\frac{1}{1 + j\omega R_f C} = \frac{-100}{1 + j\omega 5}$$

DC drift referenced to input $< 5\ \mu V/^{\circ}C$

All thermocouple measurements were referenced to a 0 °C reference junction. Each probe was calibrated through the amplifier circuit and chart recorder, thus eliminating any error due to a zero offset on the amplifier and/or recorder.

The following schematic diagram presents the layout used in measuring the plume temperatures.

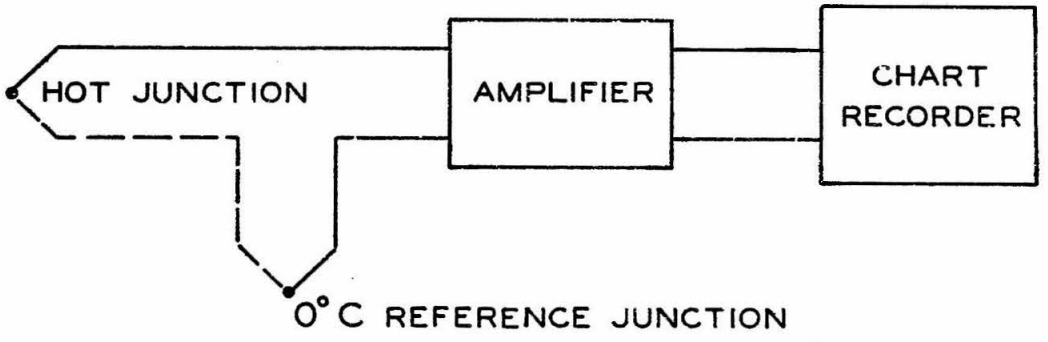

The thermocouple probe was mounted on a traversing mechanism, enabling temperature measurements at any position in the plume.

A time average of the recorded temperatures at each position was used as the mean plume temperature (a function of position).

2. Ceiling Jet Temperature Measurements. For the purpose of obtaining the ceiling jet temperature distribution, a rake consisting of 8 thermocouple probes as described above was used (see sketch below). Large temperature gradients close to the ceiling, observed during preliminary measurements, necessitated a closer spacing of thermocouple probes in the upper part of the rake. This rake was mounted on a traversing mechanism, and by traversing radially inward and outward directly underneath the ceiling, the ceiling jet

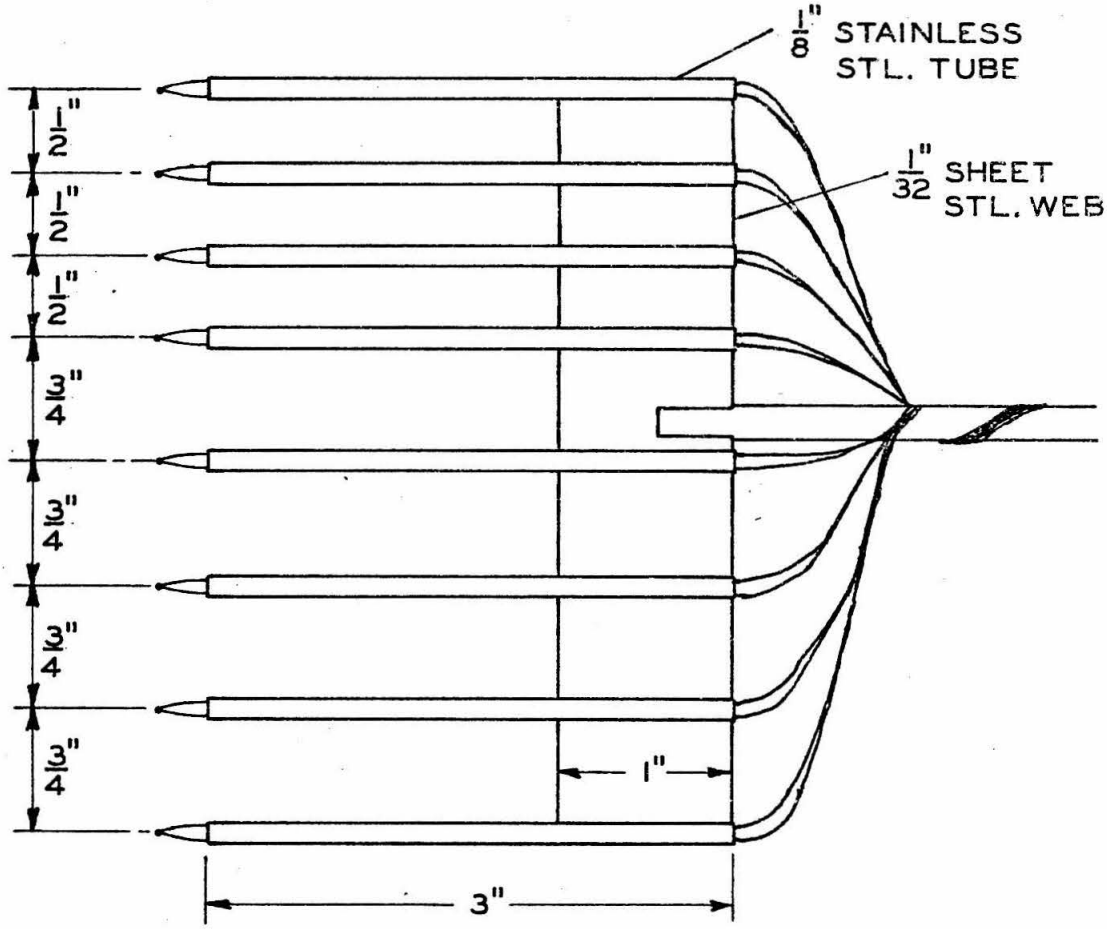

Thermocouple Rake

temperature distribution was obtained.

It was also observed during preliminary measurements that, although of lesser magnitude than in the plume, the ceiling jet temperatures also exhibited a fluctuating behavior due to turbulent flow characteristics. Since temperature measurements in the upper layers of the ceiling jet were done at distances $\frac{1}{2}$" apart, it was desirable to record at least two adjacent thermocouples simultaneously. This would also be of help in determining the nature of these fluctuations and the depth of penetration. Through the use of a second re-

corder and a switching circuit, each pair of thermocouples was recorded simultaneously. To ensure agreement of the recorded data, each set of thermocouples was calibrated through its own recording channel.

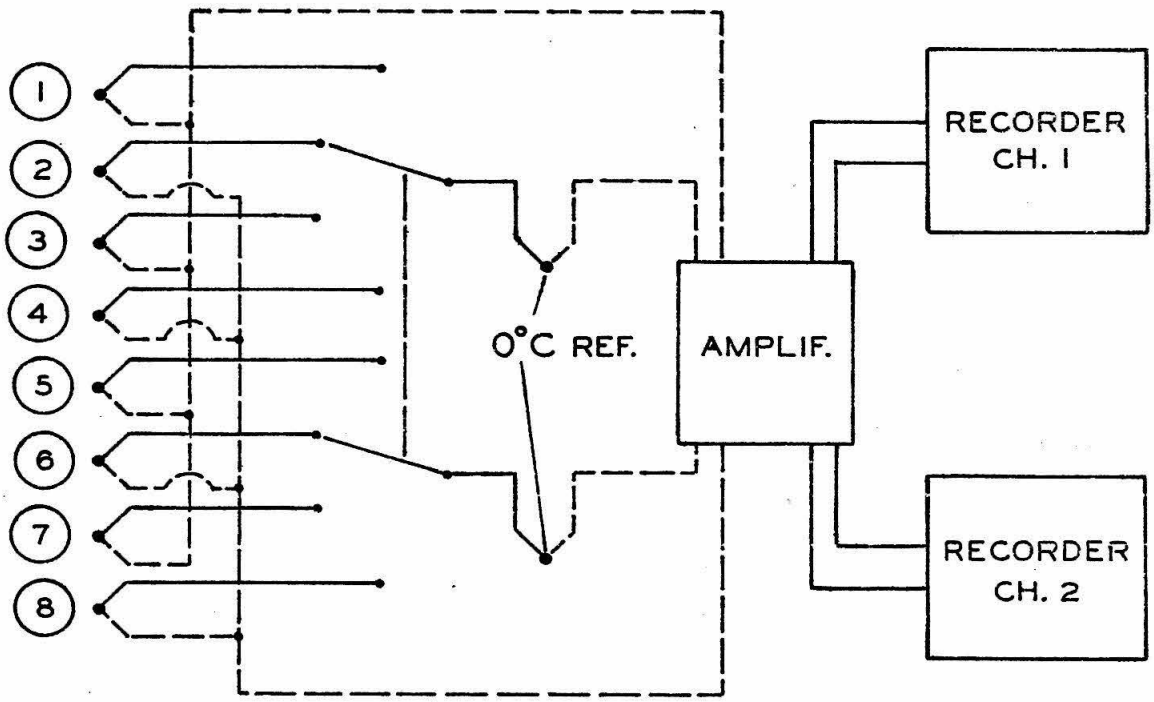

Circuit Diagram for Ceiling Jet Temperature Measurement

3. Ceiling Temperature Measurements. Ceiling temperatures were measured by thermocouple junctions spot welded onto the upper side of the ceiling, at the required radial positions, on three radii spaced 120° apart. In order to reduce the effect on the local temperature measurement of heat conducted away through the thermocouple leads, it was decided to use the same .005" diameter iron-constantan wire used for the gas temperature measurements. The use of these

small diameter wires had the added advantage that, after spot welding the junction onto the ceiling, there was practically no increase in the local thermal capacity due to added material, thus assuring a reliable measure of the local ceiling temperature. In addition, these thermocouple leads were spread out tangentially on the plate for at least a distance of 1" from the junction to further reduce the effect of conduction losses through the wire. In Appendix C it is shown that the conduction effect is indeed negligible in this case.

The problem of recording these different temperatures was overcome by using a telephone switch having 44 different switch positions. The switch was activated by a solenoid mechanism, driven by a square-wave generator with adjustable frequency.

The gas temperature in the ceiling jet was measured by a thermocouple junction underneath each corresponding position of ceiling temperature measurement (see Section II. E). These thermocouple junctions were combined with those on the ceiling in a sequence such that the ceiling temperature and corresponding gas temperature were recorded consecutively. Trial runs showed that a duration of 1 sec per temperature measurement for both the ceiling and ceiling jet was adequate. In this way, these two temperatures could be recorded almost simultaneously for each position on the ceiling, at regular intervals of 44 seconds.

It must be noted that during these measurements the filtering circuit of the amplifier could not be used, due to the characteristic time constant associated with the circuit. Although fluctuations in the ceiling jet temperature were still present, the amplitude of these

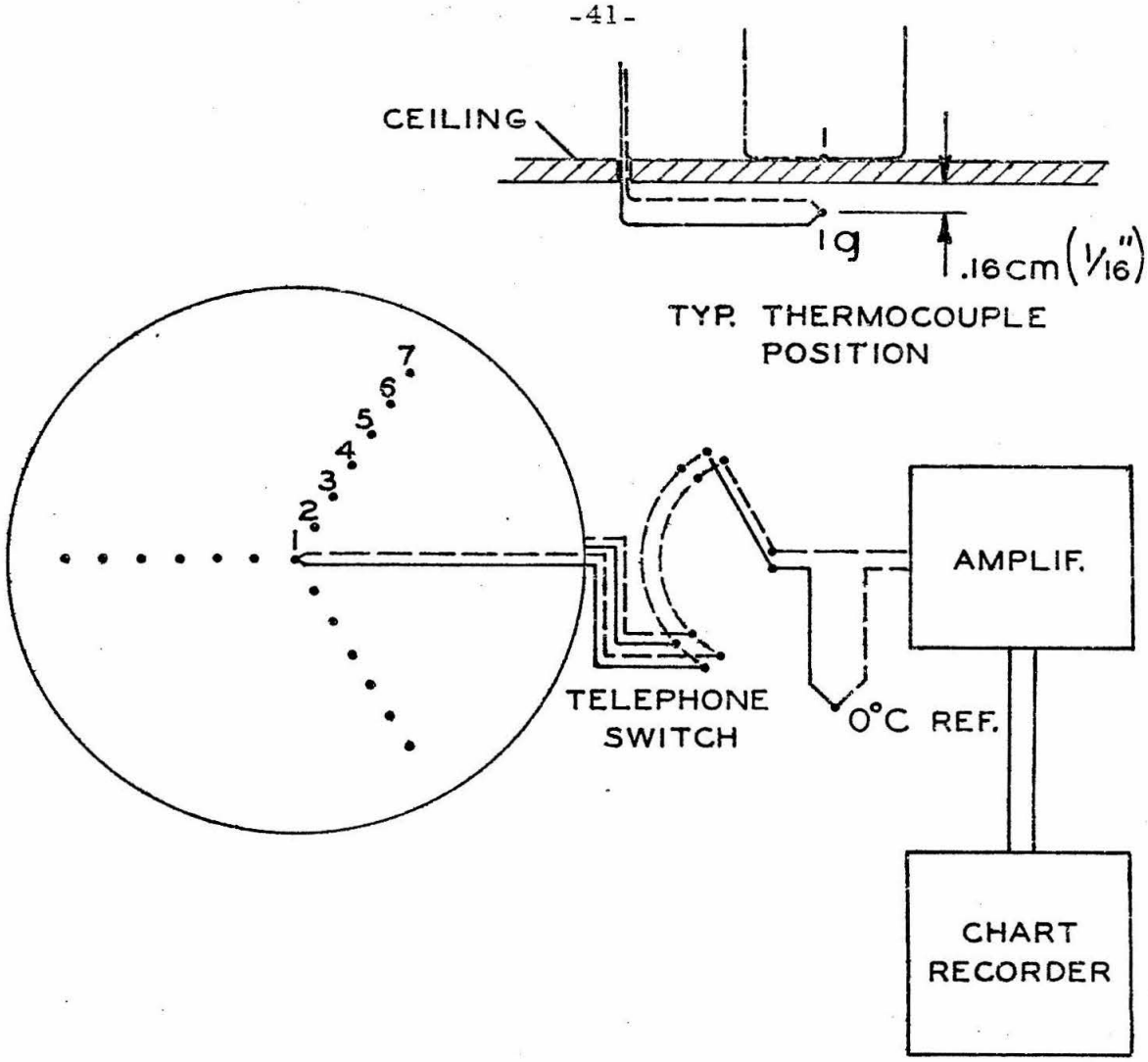

Schematic Layout for Ceiling Temperature Measurement

fluctuations adjacent to the ceiling was smaller and hence a reasonably accurate time average could be taken over a period of 1 second.

By means of this switching circuit, the temperature at each position on the ceiling was measured every 44 sec, each position being measured at a different time, according to the sequence of switching. In the reduction of the obtained data, the instantaneous temperature at all positions on the ceiling could be obtained by inter-

polation.

Shown above is a schematic layout of the circuit described, indicating the positions of ceiling temperature measurement.

IV. RESULTS AND DISCUSSION

A. Plume Temperature Distribution

As mentioned in Section II. C, mean temperatures in the undisturbed buoyant plume were determined for the purpose of defining and characterizing this specific plume, and also for comparison with results obtained by investigators such as Yokoi[2].

Although higher frequency temperature fluctuations were filtered (see Section III. B) to simplify the time-averaging procedure used for obtaining the mean temperature at each position, there was evidence of low frequency temperature variations ($\sim$ 0. 5 to 2 cycles/min), apparently due to deviations of the plume as a whole from the centerline. Though all doors and ventilation inlets of the room in which the experiment was performed were sealed and care was taken by the experimenters to cause as little motion of the surrounding air as possible, this apparent motion of the plume could not be totally eliminated. It was also found that the plume had a tendency to move over to one side with an increase in elevation above the source, possibly due to some undetected draft.

In general, however, the plume was found to be reasonably symmetric about the centerline of maximum temperature. Visualization of the plume by means of the shadowgraph method also showed no evidence of large scale deviations from the extended burner centerline. In addition, this shadowgraph method also visualized the turbulent nature of the buoyant plume and indeed confirmed that the plume was fully turbulent.

1. Radial Temperature Distribution. The radial temperature distribution at various heights above the heat source was obtained by means of the thermocouple probe described in Section III. B. Typical plume temperature data as recorded by the chart recorder are presented in Figure 2, where the magnitude of the temperature fluctuations is shown for various heights above the heat source (source strength $Q \simeq 1.17$ kW).

Despite the use of the filtering circuit, large fluctuations still occurred in the recorded plume temperatures, with the fluctuations on the centerline of the plume varying from ~ 40 per cent (at $z = 36.6$ cm) to less than 15 per cent (at $z = 101.6$ cm) of the mean value. However, repeated measurements over sufficiently long periods of time made it possible to perform time averaging and thus determine mean temperatures.

Figure 3 presents the normalized mean radial temperature data obtained at various heights above the heat source. It shows a fair agreement with the Gaussian distribution suggested by theory, and confirmed by Yokoi[2], Morton and Taylor[5], and others.

2. Centerline (Maximum) Temperature Distribution. The centerline or maximum temperature variation as a function of the elevation above the heat source was obtained from the radial temperature measurements performed at various heights. These maximum mean temperatures defined the actual centerline of the buoyant plume. Although evidence of a tendency of the plume to move over to one side was present, the actual centerline deviated less than 2.5 cm from the extended burner centerline at an elevation $z =$

100 cm. The radial and centerline absolute temperature variations are presented in Figure 4 for the case of a heat source strength Q = 1.17 kW.

Yokoi, on page 39 of ref. 2, derived an analytical expression for the maximum excess plume temperature, resulting from a circular heat source of finite radius r_o, assuming a temperature variation proportional to $z^{-5/3}$ (as verified experimentally by several investigators): refer to Section II. C. 1.

$$\Delta T_{max} = 0.423 \sqrt[3]{\frac{T_o Q^2}{C_p^2 \rho^2 g}} \; c^{-8/9} \; z^{-5/3} \quad , \qquad (4.1)$$

where $c^{2/3} = 0.1$, derived from laboratory experiments.

To compare the plume generated by the gas burner used in these experiments with those generated by alcohol pan fires used by Yokoi, the values pertaining to these experiments are substituted into eqn. (4.1) (see Table I). For $z = 20'' = 0.508$ m and $Q = 1.17$ kW,

$$\Delta T_{max} = 87.1\,^{\circ}C \quad .$$

Hence, according to Yokoi, at elevations sufficiently far above the heat source, the maximum plume temperature should vary according to $z^{-5/3}$, passing through $\Delta T_{max} = 87.1\,^{\circ}C$ at $z = 20''$. Figure 5 represents the data obtained during two different experiments. In both cases, the data agree remarkably well with Yokoi's prediction, although an entirely different type of heat source was used. This confirms the fact that at elevations sufficiently removed from the source, the plume behaves independent of the source. The deviation from the predicted value at $z = 14''$ is as expected for lower elevations, due to the momentum flux becoming more important.

The fact that in the region sufficiently far from the source the plume behaves independent of the source, is also confirmed by comparing values of the source concentration Q/D^2 used by Yokoi with those used during these experiments. Yokoi used larger diameter heat sources, resulting in relatively low values of Q/D^2, ranging from 6.50 to 8.33 cal/cm^{2}sec, whereas the more concentrated heat source used during this investigation yielded concentrations of 173.4 and 226.7 cal/cm^{2}sec. Despite this large ratio in source concentrations (20 to 35), there is still a very good agreement of plume characteristics for the region "sufficiently far" from the source.

From the normalized radial temperature distribution (see Figure 3), using the Gaussian width at different heights, the plume width is shown to extrapolate to a virtual origin located in the vicinity of the center of the heat source (Figure 4). This agrees with the conclusion at which Yokoi arrives (page 45 of ref. 2).

3. Plume Spread. In the development of the appropriate scaling parameters for the buoyant plume (see Section II. C. 1), the assumption was made that the plume is straight edged, which implies a linear rate of plume spread. Measured plume temperatures proved this assumption to be valid, as is shown in Figure 4 and presented in Table II. The average value of the plume width was 0.128 z.

Alpert[1] predicts a value of $b/z = 0.138$, using an experimentally determined constant entrainment parameter. Yokoi[2] also predicts a value of $b/z = 0.138$, and confirms this with experimental data for finite diameter heat sources. The value measured here is thus 10 per cent below these estimates.

In view of the above results it can be concluded that the buoyant plume generated by the heat source used during this experimental investigation is representative of that generated by a source of buoyancy only, e. g. a floor-level fire. Hence, it serves as an acceptable model for investigating the heat transfer from a buoyant plume to a ceiling.

B. Ceiling Jet Temperature Distribution

Temperatures in the unobstructed ceiling jet were measured with the rake described in Section III. B, and also during the actual heat transfer experiments by thermocouple junctions adjacent to the ceiling at each corresponding position of ceiling temperature measurement.

The thermocouple rake was positioned such that the upper thermocouple junction was 0. 16 cm (1/16") away from the ceiling. By means of a traversing mechanism the rake could be moved radially inward and outward to the desired position.

These temperature measurements were aimed at obtaining the following information:

i) general vertical temperature profile at any radial position;

ii) development of the thermal boundary layer on the ceiling and distance below the ceiling where maximum temperature occurs;

(iii) relation between decrease in the ceiling jet maximum temperature and the increase in radius.

1. Vertical Temperature Profile. Although the temperatures in the ceiling jet were still of a fluctuating nature requiring the

use of the filtering circuit, there was a distinct decrease in the magnitude of these fluctuations compared to that in the buoyant plume. At a ceiling height of 81.3 cm, the maximum amplitude of the ceiling jet temperature fluctuations (measured at r = 14 cm and y ≃ 4 cm below the ceiling) was approximately 15 - 20 per cent of the mean value as opposed to 25 - 30 per cent for the plume centerline temperature fluctuations at the corresponding height. This reduction was as expected, due to

i) the presence of a solid boundary (the ceiling itself);

ii) a decrease in the maximum temperature with an increase in radius;

iii) the stratified nature of the ceiling jet, i.e., the hot gas is bounded by the ceiling from above and by layers of cooler, more dense, air from below.

Temperature measurements were carried out at different radial positions, after a steady state was reached, i.e., when the ceiling temperature reached a constant value (this occurred after 25 to 30 min). These measurements were also done for two different strengths of the heat source (Q = 1.17 kW and 1.53 kW). For each radial position, the temperatures were normalized by the corresponding maximum temperature. The measured temperature profiles shown in Figure 6 agreed very well with the Gaussian profile suggested by theory and verified experimentally by Alpert[1] and others.

The thickness of the ceiling jet, based on the temperature measurements, is characterized by the Gaussian width ℓ. Since, in these experiments, $r/H < 0.7$, the variation in ceiling jet thickness

with radius was not distinct, although at both heating rates it appeared that the value of b increased from about 3.5 cm (1.4") at r/H = 0.22, to 4 cm (1.6") (Q = 1.17 kW), and to 4.8 cm (1.9") (Q = 1.53 kW) at r/H = 0.47. For further information about the ceiling jet thickness variation, it is essential to do at least some velocity measurements to determine the thickness of the velocity boundary layer (see Alpert[1]). Such velocity measurements were not permitted during the course of these experiments due to time limitations.

From these vertical temperature measurements it is possible to determine the radial plane where the ceiling jet left the turning region (or stagnation point). For both heating rates this occurred at between r = 10.2 cm (4") and r = 12.7 cm (5"), which corresponds to the diameter of the plume at a height of 76.2 cm (30") to 81.3 cm (32").

2. Development of the Thermal Boundary Layer. During a second series of ceiling jet temperature measurements, the thermocouple rake was positioned at a radial distance r = 28 cm (11") from the centerline, where it was held fixed while the temperature distribution through the jet was obtained at regular intervals for a period of 30 minutes after the burner was started.

The absolute temperatures measured during this period were plotted against the distance from the ceiling, y , for different times. The results are presented in Figure 7. From these plots, the development of the thermal boundary layer on the ceiling is obvious. In the early stages of the experiment, up to approximately 176 sec, the temperature adjacent to the wall remained nearly constant, with

a very distinct thermal boundary layer due to heat transfer to the ceiling. The maximum ceiling jet temperature occurred at a distance of 1 cm to 1.3 cm below the ceiling.

Between 176 sec and 352 sec, the temperature adjacent to the ceiling started increasing, corresponding to a decrease in the ceiling heat transfer. After approximately 20 minutes the maximum temperature occurred adjacent to the ceiling with no evidence of a thermal boundary layer. This indicated the existence of an "adiabatic wall" condition. There was a slight increase in this maximum temperature after 30 minutes, but the temperature profile retained its shape. The apparent increase in the temperatures in the lower part of the ceiling layer after 30 minutes is misleading, since it was caused by a local fluctuation occurring at that instance, possibly due to movement of the whole plume.

Based on the general shape of these temperature profiles, it was decided to use two thermocouple junctions to obtain the ceiling jet temperature at each radial position during the heat transfer measurements;

i) one thermocuople adjacent to the wall at a distance y = 1/16", to measure the adiabatic wall temperature;

ii) a second thermocouple at y = 3/8", to measure the local maximum temperature occurring during the early stages when the heat transfer data are taken (refer to Section IV. B).

3. Radial Maximum Temperature Distribution. The variation in the maximum ceiling jet temperature as a function of the

radius was obtained during the heat transfer experiments by means of a thermocouple junction 1/16" away from the ceiling at each radial position where the ceiling temperature was measured. The results of one such measurement of the "adiabatic wall" temperature are shown in Figure 8, for a source strength Q = 1.17 kW and a ceiling height H = 0.813 m (32"). Because heat transfer to the ceiling is virtually zero, the decrease in temperature shown in this figure is due to entrainment of cold air by the ceiling jet. There is no evidence of a hydraulic jump in the ceiling layer at any radius.

It is useful to present these temperatures in the dimensionless form as a function of the dimensionless radial position which was suggested in Section II. D:

$$\frac{\Delta T_{ad}/T_\infty}{(Q^*)^{2/3}} = f_1\left(\frac{r}{H}\right) . \tag{2.29}$$

The values of Q, H, Q^*, and ambient conditions used during the experiments are listed in Table I. Substitution of the respective values into eqn. (2.29) yields:

(a) Test No. 1

$$\frac{\Delta T_{ad}}{4.354} = f_1\left(\frac{r}{H}\right) \tag{4.2}$$

(b) Test No. 2

$$\frac{\Delta T_{ad}}{5.207} = f_1\left(\frac{r}{H}\right) \tag{4.3}$$

(c) Test No. 3

$$\frac{\Delta T_{ad}}{7.558} = f_1\left(\frac{r}{H}\right) \tag{4.4}$$

The adiabatic ceiling jet temperatures measured during the three different heat transfer experiments are non-dimensionalized according to eqns. (4.2) to (4.4), and the results are presented in Figure 9 (see also Table III). Also shown in this figure is the theoretical curve for a Gaussian profile ceiling jet temperature, as obtained by Alpert[1], as well as two sets of data points obtained by the latter (see page 86 of ref. 1).

Equations (4.2) to (4.4) represent a change of a factor of 1.74 in the maximum ceiling jet temperature parameter. This is a large factor compared to the scatter of data in Figure 9. The good agreement between the data of these various experiments confirms the validity of this parameter for the range covered by Q and H.

Some data are available which appear to extend the validity of this correlation over a considerably wider range. Data from refs. 11 and 12 (taken from Alpert[1], Fig. 7, page 80) are shown in Figure 10, where they are compared with the data shown in Figure 9. However, it is not clear what is meant by the "near-maximum, excess ceiling-jet temperature", though this temperature must lie within the range ΔT_{max} and $1/\sqrt{2}\ \Delta T_{max}$. For this reason, the average data obtained by the author are presented by two curves. This correlation suggests that the entrainment in the ceiling jet, as well as the plume which furnishes the initial ceiling jet temperature, scale properly over a much wider range of Q^* (see tabulated values of Q^* on Figure 10).

According to Figure 9, $(\Delta T_{ad}/T_\infty)/(Q^*)^{2/3}$ assumes a value between 9.5 and 10 at $r = 0$. The corresponding value of this pa-

rameter for the unobstructed plume (Figure 5) is 9.11 (also see Sections II. C and IV. D). The slightly higher value in the case of the ceiling jet is expected, since in the presence of the ceiling a turning region exists with less entrainment in the plume in this region than would have been the case without the ceiling. This should result in a slightly larger value of the plume centerline temperature, as confirmed by Figure 9. Thus, the equality of these two temperature parameters at $r = 0$ confirms the validity of the assumption made in the derivation of the model for the ceiling jet, in which it was assumed that the ceiling jet starts out with the maximum plume temperature taken at the corresponding height.

The fast decrease in this adiabatic ceiling jet temperature with an increase in radius, in the absence of heat transfer to the ceiling, is caused by the entrainment of air into the ceiling jet. In his study of the ceiling jet, Alpert[1] shows the entrainment velocity u_{ent} to be a function of an entrainment parameter E_j (assumed constant), the average ceiling jet velocity V, and to depend exponentially upon the Richardson number Ri. However, for $r/H < 1$, the dependence on Ri is negligible, thus resulting in a constant entrainment velocity $u_{ent} \simeq 0.1\,V$. As shown in Figure 9, the experimental data tend to flatten out in the turning region (stagnation region); whereas in the ceiling jet, although generally somewhat lower than the predicted value, there is a good agreement with the theoretical curve. However, since the dependence on E_j is not very strong, this was not a critical test.

Judging from these results, the dimensionless parameter for

the adiabatic ceiling jet temperature (eqn. (2.29)) seems appropriate for the range of heat inputs and ceiling heights covered during this experimental investigation. This yields a very useful method of estimating the maximum temperature to be expected in a ceiling jet under an "adiabatic" ceiling condition for a given strength of heat source (Q) and a given ceiling height (H). An estimate of this temperature makes it possible to estimate the ceiling heat transfer under these conditions (see next section).

C. Ceiling Heat Transfer

1. General Discussion. The heat transferred from the buoyant plume and ceiling jet to the unobstructed ceiling was investigated for three different cases (see Table I). In each case, prior to starting the experiment, the ceiling had a uniform initial temperature equal to the ambient temperature. The gas burner was then started without causing any motion of the surrounding air, and the stepping switch for registering ceiling and ceiling jet temperatures was actuated simultaneously. Temperatures were measured continuously for a period of 8 minutes. Thereafter temperatures were measured at 5-minute intervals. In all cases, an "adiabatic wall" condition was established after 25 to 30 minutes, at which time the experiment was terminated.

The values of the properties of the air, ceiling, and insulation used in the calculation of the heat transfer rates are presented in Table I. The ceiling consisted of a 1/16" cold-rolled steel plate ($\simeq$ 1 per cent carbon content), and was supported at four positions such that the conduction losses through these supports were negligible.

2. Ceiling Heat Transfer (q_c). The ceiling heat transfer per unit area (q_c) was obtained by considering the increase in ceiling internal energy, and applying corrections for losses through radial conduction and through the backing insulator (refer to eqn. (2.31)).

a) Increase in ceiling internal energy (ΔE). By considering the slope of the temperature history curve at each position on the ceiling, the increase in internal energy of the ceiling was obtained according to eqn. (2.32):

$$\Delta E(r,t) = 5858 \left.\frac{\partial T}{\partial t}\right|_{r,t} \qquad (W/m^2) \qquad (4.5)$$

The temperature histories for four different radial positions as recorded during Test No. 1 are presented in Figure 11. In all cases, the temperature curves were very smooth, thus enabling a good estimate of the slope $\partial T/\partial t$, at each required time. The results for each experiment are given in Tables VII, VIII, and IX, respectively.

b) Radial conduction correction (q_{cond}). As discussed in Section II.E, the correction for the heat loss through radial conduction along the ceiling given by eqn. (2.34) is

$$q_{cond}(r,t) = -2735 \left.\frac{\partial}{\partial(r^2)}\left(r^2 \frac{\partial T}{\partial(r^2)}\right)\right|_{r,t} \qquad \text{(for } r \text{ in cm)} \quad (4.6)$$

For positions 1 and 2 (i.e., r = 0 and r = 7 cm), graphical evaluation of the second derivative $\frac{\partial}{\partial(r^2)}\left(r^2 \frac{\partial T}{\partial(r^2)}\right)$ was impossible and therefore an analytical evaluation of q_{cond} was used. For the remaining radial positions, graphical evaluation proved to be acceptable. From the results (presented in Tables VII - IX), the importance of

the radial conduction term at r = 0 and r = 7 cm is clear. At r = 0, q_{cond} assumed the same magnitude as ΔE within 3 to 5 minutes after starting, and was the dominating term after 7 minutes. The same kind of behavior was observed at r = 7 cm, though of smaller magnitude. This region on the ceiling coincides with the region of plume impingement (stagnation region) and the rapid increase in the value of $r^2 \frac{\partial T}{\partial (r^2)}$ from 0 at r = 0 leads to a large value for the second derivative in this region. Thus, an appreciable error in the value of q_{cond} (and hence of q_c) has to be expected for this region.

For radial positions located at values of r in excess of 7 cm, the radial conduction term was at least an order of magnitude smaller than ΔE, and only after 7 minutes did it contribute approximately 10 per cent to the final value of q_c.

c) Heat loss through backing insulator (q_{loss}). The heat loss through the insulation material can be estimated by eqn. (2.46) (see Section III.E):

$$q_{loss}(r,t) = 24.0 \sqrt{t} \sum_{n=0}^{\infty} a_n c_n t^n , \tag{4.7}$$

where

$$\begin{aligned} T'_{ins} &= T'_c(r,t) = a_o + a_1 t + a_2 t^2 + a_3 t^3 + a_4 t^4 \\ c_o &= 1 \; ; \; c_1 = 0.667 \; ; \; c_2 = 0.533 \; ; \\ c_3 &= 0.457 \; ; \; c_4 = 0.406 \; . \end{aligned} \tag{4.7a}$$

With the temperature history of the ceiling known, and under the assumption that the surface of the insulation in contact with the ceiling has the same temperature as the ceiling, a least-squares fit of a fourth degree polynomial was used to evaluate the coefficients in

eqn. (4.7a). The results are presented in Tables VII - IX. From these tables it can be seen that the magnitudes of these losses are much less than that of ΔE and q_c. In the region r = 0 to r = 14 cm, the value of q_{loss} was almost constant, whereas in the outer region it increased during the first 5 minutes; thereafter it tended to stabilize.

Substituting the above values for ΔE, q_{cond}, and q_{loss} into eqn. (2.31) yielded the actual rate of heat transfer to the ceiling as a function of radius and time (refer to Tables VII, VIII, and IX). In Figure 12 the variation in q_c as a function of radius can be seen for the three different experiments (at time t = 2 min).

A very drastic decrease in q_c with an increase in radius occurred at t = 1 min, with q_c at r = 42 cm (outer position) approximately 8 - 10 per cent of that at r = 0. Due to the increase in ceiling temperature T_c with time, the heat transfer rate decreased with time. After 7 minutes, $q_c(r = 0)$ had decreased between 50 and 60 per cent; whereas at r = 42 cm, q_c decreased only by 30 - 40 per cent.

With the values of $q_c(r, t)$ known, an estimate was made of the ratio of total ceiling heat transfer to the heat supplied by the source. This was done as follows. For t = constant, let

$$q_c(r) = b_o + b_1 r + b_2 r^2 + b_3 r^3 + b_4 r^4$$

(fourth degree polynomial fitted to the obtained values of $q_c(r)$ at 7 radial positions).

Then, the total rate of heat transfer to the ceiling is:

$$Q_c = \int_0^R q_c(r)\, 2\pi r\, dr \ .$$

$$\therefore\ Q_c = 2\pi R^2 \left[\frac{1}{2} b_o + \frac{1}{3} b_1 R + \frac{1}{4} b_2 R^2 + \frac{1}{5} b_3 R^3 + \frac{1}{6} b_4 R^4\right] , \qquad (4.8)$$

where $R = 18'' = 45.7$ cm.

The results are presented in Table X. Surprisingly, a maximum of only 18 - 20 per cent of the heat supplied by the source was transferred to the ceiling at $t = 1$ min , and this value decreased to 7 - 10 per cent after 7 minutes. This suggests a large entrainment of cooler ambient air in both the plume and ceiling jet, as was evidenced by the decrease of these maximum temperatures (see Sections IV. A and IV. B). The increase in Q_c/Q with a decrease in H was as expected, since less entrainment occurred in the shorter plume; thus, a larger temperature gradient is available to drive the heat transfer to the ceiling.

In a confined space, e. g. a closed room, this will only be the case in the initial stages, since eventually all the air in the room will be heated and hence more heat will be available to increase the ceiling temperature.

3. Ceiling Heat Transfer Coefficient (h_c). The ceiling heat transfer coefficient, h_c, is defined by eqn. (2.47) as $q_c/\Delta T$ ($W/m^2\ ^oK$). During the first experiment, both the adiabatic ceiling temperature adjacent to the wall (reached after 25 - 30 min) and the local maximum ceiling jet temperature, corresponding to the time at which the ceiling heat transfer was obtained, were measured. Whereas determining the "adiabatic" ceiling jet temperature presented little or no problems, uncertainty existed about the distance away from the

ceiling where the local maximum temperature occurred (ceiling jet temperature profiles indicated this maximum to occur between 1.0 and 1.3 cm below the ceiling). A second thermocouple junction was therefore positioned in this region (see Figure 7). Local temperature fluctuations in this region, however, influenced the accuracy of these measurements and was suspected to be responsible for a substantial error in the heat transfer coefficient $h_{c_{local}}$, based on this temperature, especially after 5 to 7 minutes when the increased ceiling temperature reduced ΔT to a value which could easily be off by a factor of ± 50 per cent, due to a local fluctuation occurring at the time the data were taken.

In all experiments, a steady state was reached after 25 - 30 minutes, with the ceiling temperature (at each position) approaching a constant value asymptotically, and with the maximum ceiling jet temperature occurring adjacent to the wall. This indicated the existence of an "adiabatic wall" condition. Though such a steady state was reached, it was found that at positions r = 0 and r = 7 cm, the ceiling temperature was approximately 5 - 10 ^{o}C lower than that of the ceiling jet, indicating that some heat transfer still occurred to the ceiling. This was due to the large component of radial conduction along the ceiling in this region, which still existed due to the steady radial temperature gradient. A comparison between the heat transfer coefficient based on the local maximum ceiling jet temperature ($h_{c_{local}}$) and that based on the adiabatic ceiling jet temperature ($h_{c_{ad}}$) (see Figure 13) shows the odd behavior of $h_{c_{local}}$ after 5 minutes. As a result of these observations, the ceiling heat transfer

coefficient was based on the difference between the adiabatic ceiling jet temperature and the ceiling temperature, i.e.,

$$h_c(r,t) = \frac{q_c}{\Delta T_{ad}} \quad . \tag{4.9}$$

The experimental results are presented in Tables XI, XII and XIII.

4. Dimensionless Ceiling Heat Transfer Coefficient. The non-dimensionalizing of the ceiling heat transfer coefficient is discussed in Section II. E, and has the form:

$$\frac{h_c}{\rho_\infty C_p \sqrt{gH}\,(Q^*)^{1/3}} = h_c' = f_2\left(\frac{r}{H}\right) \quad , \tag{2.53}$$

where

$$Q^* = \frac{Q}{\rho_\infty C_p T_\infty \sqrt{gH}\, H^2} \quad .$$

Substitution of the values of Q, H, Q^* and ambient conditions pertaining to each experiment (see Table I) yields the following expressions for eqn. (2.53):

Test No. 1

$$\frac{h_c}{405.2} = f_2(r/H) \tag{4.10}$$

Test No. 2

$$\frac{h_c}{450.6} = f_2(r/H) \tag{4.11}$$

Test No. 3

$$\frac{h_c}{443.0} = f_2(r/H) \tag{4.12}$$

The experimental results are presented in Tables XIV, XV, and XVI. In Figure 14 the variation of h_c' as a function of r/H is shown for the above three tests at times t = 2, 3, and 5 minutes.

Also shown in this figure are two theoretical curves obtained by Alpert[1], as well as one set of data points derived from experiments by the latter.

The theoretical curves are based on a Stanton number obtained by applying the Reynolds analogy between heat transfer and fluid friction for fully turbulent flow, i.e.,

$$\frac{h_c}{\rho V C_p} = Pr^{-2/3} f/2 \quad . \tag{4.13}$$

In this analysis, Alpert based h_c on a "mean flow temperature." Assuming a Gaussian velocity and density (temperature) profile, the mean temperature is $1/\sqrt{2}$ times the maximum temperature. Therefore, in order to correlate h_c obtained by the above mentioned with that of the author, Alpert's values of h_c are reduced by a factor $\sqrt{2}$. The same applies to the theoretical curves.

Although eqns. (4.10) to (4.12) show only a factor 1.11 variation in the parameter for the ceiling heat transfer coefficient, there is a considerable scatter of data as shown in Figure 14, mainly due to limitations on the accuracy of experimental results and also due to errors in the correction for the radial conduction along the ceiling (as discussed in a previous section).

Substitution of the values for Q and H used by Alpert during his experiments yields $h_c/336.2 = f_2(r/H)$. This differs by a factor 1.34 from the value given by eqn. (4.11). As can be seen in Figure 14, Alpert's data points lie within the scatter of data obtained by the author, thus supporting the suggested form for the dimensionless heat transfer coefficient as given by eqn. (2.53). The scatter of data in

Figure 14 is bounded by the theoretical curves for $f = 0.02$ and 0.04, which implies a fair agreement with the predicted values.

5. Estimating Ceiling Heat Transfer and Temperature Increase. With the information obtained during this experimental investigation, it is possible to estimate the heat transfer to and resulting temperature increase of an unobstructed ceiling for given values of Q and H in the region $r/H < 0.7$. The following steps outline such an estimate.

i) At $t = 0$, $T_c = T_\infty$ and therefore $\Delta T_{ad} = T_{ad} - T_\infty$. The value of ΔT_{max} as a function of radius can be obtained from Figure 9.

ii) Values for $h_{c_{ad}}$ can be taken from Figure 14.

iii) The ceiling heat transfer as a function of radius can now be calculated from

$$q_c(r)\Big|_{t=0} = h_c \Delta T_{ad} \quad . \tag{4.14}$$

iv) Now, by taking an increment in time Δt, the ceiling temperature at $t = t_1$ can be estimated from

$$\Delta T_c(t_1) = \frac{q_c \Delta t}{\rho \delta C} - q_{loss} \quad . \tag{4.15}$$

In the case of a ceiling with low conductivity, the term q_{loss} will be small and can be neglected as a first approximation.

v) With this value of ΔT_c, a new value for $\Delta T_{ad} = \Delta T_{ad} - \Delta T_c$ can be obtained, and substitution into (4.14) yields a new value for $q_{c_{t=t_1}}(r)$.

vi) This process can now be repeated by each time incrementing the time by Δt.

D. Summary of Correlations

This section serves as a compact summary of the correlations for the parameters and variables governing the heat transfer from a buoyant plume to an unobstructed horizontal ceiling. The constants specified here are the experimentally obtained results of the author as well as other investigators such as Alpert[1] and Yokoi[2].

1. Buoyant Plume

$$Q^*\{z\} = \frac{Q}{\rho_\infty C_p T_\infty \sqrt{gz}\, z^2}$$

$$\frac{\Delta T_{max}}{T_\infty} \simeq 9.11 (Q^*\{z\})^{2/3}$$

$$\frac{V}{\sqrt{gz}} \simeq 3.87 (Q^*\{z\})^{1/3}$$

$$b/z \simeq 0.138$$

2. Ceiling Jet

$$Q^*\{H\} = \frac{Q}{\rho_\infty C_p T_\infty \sqrt{gH}\, H^2}$$

$$\frac{\Delta T_{ad}}{T_\infty} = f_1(r/H)(Q^*\{H\})^{2/3} \qquad (2.29)$$

See Figure 9 or 10.

3. Ceiling Heat Transfer

i)
$$\frac{h_c}{\rho_\infty C_p \sqrt{gH}} = f_2(r/H)(Q^*\{H\})^{1/3} \qquad (2.53)$$

See Figure 14.

ii) Time scale , for thin slab ceiling initially at T_∞ :

$$\frac{\Delta T_c}{\Delta T_{ad}} = \frac{T_c - T_\infty}{T_{ad} - T_\infty} = 1 - \frac{1}{e}$$

when

$$\frac{t_c\sqrt{gH}}{\delta} = \left(\frac{\rho_c C_c}{\rho_\infty C_{p_\infty}}\right)(Q^*\{H\})^{1/3}\left[f_2\left(\frac{r}{H}\right)\right]^{-1} \qquad (2.61)$$

As an example of the application of the above experimentally-determined values for the temperature and heat transfer parameters, calculations were carried out for the case of a much larger heat source (200 kW), a ceiling height of 1.825 m, and a 1/2" thick plasterboard ceiling -- comparable to a normal room condition.

The calculations were done for the position r = 0. The results are presented in Table XVII, where it is also compared with that of one experimental case (Q = 1.17 kW and H = 0.584 m). From this table it can be seen that an increase by a factor of 200 in the heat source strength only results in a factor of 5 increase in the maximum plume temperature at the ceiling. However, there is a large increase in the heat transferred to the ceiling per unit area. No drastic change in the characteristic time occurs.

The factor of 10 increase in Q^* might be responsible for a substantial error in the above values, since in the experimental work Q^* only varied by a factor 2.3 (see Table I). In addition, the Reynolds number effect on f or h_c has not been taken into account here. This example might, however, serve as a very rough estimate of temperatures and heat transfer rates to be expected under large-scale room fire conditions.

V. CONCLUSIONS

1) The experimental modeling of an axisymmetric floor-level fire beneath an unobstructed ceiling was successfully accomplished by using a premixed propane gas burner with a known heat input. The resulting buoyant plume agreed well with results obtained for small-scale fires in the region far away from the heat source (approximately 10 - 15 diameters) where the initial momentum flux is dominated by the buoyancy flux.

2) The temperature occurring in a ceiling jet beneath an unobstructed adiabatic ceiling, as a function of the radial distance, can be predicted for a given heat source strength Q and a given ceiling height H as long as $H/D > 10$, where D is the diameter of the heat source.

3) An experimental model was developed for estimating the heat transfer from a buoyant plume and resulting ceiling jet to a horizontal unobstructed ceiling for a given value of the heat source strength Q and ceiling height H. The resulting rate of increase of the ceiling temperature can therefore be estimated.

The major contribution of the experimental work reported in this thesis is that it presents values of the ceiling heat transfer coefficient in an axisymmetric case for the region $0 \leq r/H \leq 0.7$. Very little such data existed and, in particular, no data existed for the stagnation region ($r/H = 0$). The heat transfer coefficient is based on the adiabatic ceiling jet temperature, which can be estimated satisfactorily for a known heat source strength and ceiling height.

REFERENCES

1. Alpert, R. L. "Fire-Induced Turbulent Ceiling-Jet," Technical Report, Factory Mutual Research Corp., FMRC Serial No. 19722-2 (May 1971).

2. Yokoi, S. "Study on the Prevention of Fire Spread Caused by Hot Upward Current," Report No. 34, Building Research Institute, Japanese Government (November 1960).

3. Gaydon, A. G. and Wolfhard, H. G. Flames -- Their Structure, Radiation and Temperature, 2nd Ed., Chapmann and Hall (London), 1960, p. 78.

4. Morgan, G. H. and Kane, W. R. "Some Effects of Inert Diluents on Flame Speeds and Temperatures," 4th Symposium (International) on Combustion, Williams and Wilkins (Baltimore), 1953, p. 319.

5. Morton, B. R., Taylor, Sir G., and Turner, J. S. "Turbulent Gravitational Convection from Maintained and Instantaneous Sources," Proc. Roy. Soc. (London), Series A, 234 (1956), pp. 1-23.

6. Rouse, H., Yih, C. S., and Humphreys, H. W. "Gravitational Convection from a Boundary Source," Tellus, 4 (1952), pp. 201-210.

7. List, E. J. and Imberger, J. "Turbulent Entrainment in Buoyant Jets and Plumes, J. Hydr. Div., Proc. Am. Soc. Civil Eng., 99, no. HY9 (September 1973).

8. Eckert, E. R. G. and Drake, R. M. Analysis of Heat and Mass Transfer, McGraw-Hill (New York), 1972.

9. Glauert, M. B. "The Wall Jet," J. Fluid Mech., 1 (1956), p. 625.

10. Bakke, P. "An Experimental Investigation of a Wall Jet," J. Fluid Mech., 2 (1957), p. 467.

11. Miller, M. J. "Progress Report on Fire Modelling," No. 14466/3218, Factory Mutual Eng. Div. (1962).

12. Thompson, N. I. "Fire Behavior and Sprinklers," National Fire Protection Association, Boston (1964).

13. Chemical Engineers' Handbook, 4th Ed., McGraw-Hill (New York), 1963.

14. McMahon, H.M. "An Experimental Investigation of the Effect of Mass Injection at the Stagnation Point of a Blunt Body," Appendix B, Memo No. 42, Guggenheim Aeronautical Lab., California Institute of Technology (May 1958), p. 70.

TABLE I. Test Conditions and Constants

	Q (kW)	H (m)	Q^*
Test No. 1	1.17	0.813	0.00181
Test No. 2	1.17	0.584	0.00413
Test No. 3	1.53	0.813	0.00236

Constants:

Air: $C_p = 1006$ Ws/kg ^oK, $\rho_\infty = 1.17$ kg/m^3 } at 295 ^oK

Ceiling: $C_c = 473$ Ws/kg ^oK

$\rho_c = 7801$ kg/m^3

$k_c = 43$ W/m ^oK

$\delta = 1.59 \times 10^{-3}$ m

Insulator: $\rho_{ins} = 10.41$ kg/m^3

$C_{ins} = 954$ J/kg ^oK

$k_{ins} = 0.046$ W/m ^oK

Constants for air and ceiling were obtained from Eckert and Drake[8].

Constants for insulation, refer to Appendix B.

TABLE II. Plume Spread

b (cm)	z (cm)	b/z
4.902	36.58	0.134
6.48	50.80	0.128
8.25	66.04	0.125
10.24	81.28	0.125
13.08	101.60	0.129

TABLE III. Dimensionless Adiabatic Ceiling Jet Temperature

Test	Pos. #	1	2	3	4	5	6	7
#1	r/H	0	.086	.172	.258	.344	.431	.517
	$\frac{\Delta T_{max}}{T^*}$	10.56	8.84	8.04	7.12	5.52	4.37	4.02
#2	r/H	0	.086	.172	.258	.344	.431	.517
	$\frac{\Delta T_{max}}{T^*}$	9.60	9.45	7.30	6.15	5.19	4.51	4.23
#3	r/H	0	.120	.240	.360	.479	.599	.719
	$\frac{\Delta T_{max}}{T^*}$	10.45	8.07	6.81	5.29	4.45	3.51	3.14

$$T^* = T_\infty (Q^*)^{2/3}$$

TABLE IV. Measured Ceiling Temperatures (^{o}C), Test No. 1

t (sec)*		0	44	88	132	176	220	264	308	352	396	440	484
Pos. #	r (cm)												
1	0	22	29.1	35.0	39.3	42.2	44.1	45.7	47.7	49.2	50.8	52.5	53.1
2	7	22	27.7	33.2	36.5	39.1	41.0	42.8	44.5	45.9	47.3	48.8	49.6
3	14	22.3	26.2	29.9	32.8	35.0	36.3	38.1	39.5	41.0	42.4	43.6	44.7
4	21	22	24.8	27.1	29.3	31.2	32.4	33.8	35.2	36.5	37.5	38.7	39.5
5	28	22	24.0	25.8	27.5	28.5	29.7	30.9	31.8	32.8	33.8	35.0	35.5
6	35	22	23.2	24.4	25.6	26.8	27.7	28.7	29.5	30.3	31.4	31.8	32.8
7	42	21.9	23.0	24.0	25.2	25.8	27.0	27.5	28.3	29.3	29.7	30.5	31.2

Initial Ceiling Temperature = 21^{o}C. Refer to Table I for Q and H .

* t is the time at which the ceiling temperatures at Position 1 were measured. The corresponding times for the other radial positions are:

Position 2 t + 3 sec.
Position 3 t + 9 sec.
Position 4 t + 16 sec.
Position 5 t + 22 sec.
Position 6 t + 29 sec.
Position 7 t + 35 sec.

TABLE V. Measured Ceiling Temperature (^{o}C), Test No. 2

t (sec)*		0	44	88	132	176	220	264	308	352	396	440	484
Pos.#	r (cm)												
1	0	21.5	34.8	44.3	50.8	55.3	59.4	63.5	66.8	68.4	71.1	72.5	73.8
2	7	21.5	30.1	37.5	43.0	47.7	51.8	55.9	58.6	60.7	63.1	64.8	66.4
3	14	21.5	26.6	31.3	35.2	39.1	42.6	45.7	48.6	50.6	52.7	54.3	55.7
4	21	21.1	24.0	27.3	29.9	32.8	35.2	37.7	40.0	41.6	43.2	44.9	46.1
5	28	20.7	22.9	24.8	26.6	28.7	30.5	32.4	33.8	35.2	36.7	37.7	39.1
6	35	20.3	21.7	23.0	24.4	25.8	27.3	28.9	29.9	31.2	32.2	33.2	34.2
7	42	20.3	21.5	22.5	23.6	25.0	26.2	27.3	28.1	29.3	30.3	31.2	32.0

Initial Ceiling Temperature = 19.3 ^{o}C. Refer to Table I for Q and H.

* t is the time at which the ceiling temperatures at Position 1 were measured. The corresponding times for the other radial positions are:

Position 2 t + 3 sec.
Position 3 t + 9 sec.
Position 4 t + 16 sec.
Position 5 t + 22 sec.
Position 6 t + 29 sec.
Position 7 t + 35 sec.

TABLE VI. Measured Ceiling Temperatures (^{o}C), Test No. 3

t (sec)*		0	44	88	132	176	220	264	308	352	396	440	484
Pos.#	r (cm)												
1	0	19.5	28.9	34.2	40.4	44.1	47.8	51.2	52.9	54.7	55.9	57.0	58.0
2	7	19.5	26.8	32.0	36.3	40.2	43.7	46.7	48.1	50.4	51.6	52.7	54.1
3	14	19.9	24.6	28.5	31.4	34.6	37.9	40.6	42.4	44.1	45.7	46.9	47.7
4	21	19.5	23.0	25.8	27.7	30.5	32.8	33.4	37.1	38.3	39.8	41.0	41.8
5	28	19.5	21.9	23.8	25.8	27.5	29.3	31.2	32.4	34.0	35.2	36.1	36.9
6	35	19.5	21.1	22.7	24.0	25.4	27.0	28.5	29.5	30.3	31.8	32.6	33.4
7	42	19.5	20.7	22.1	23.0	24.6	25.6	27.0	27.7	28.7	30.1	30.7	36.9

Initial Ceiling Temperature = 19 ^{o}C. Refer to Table I for Q and H.

*t is the time at which the ceiling temperatures at Position 1 were measured. The corresponding times for the other radial positions are:

Position 2 t + 3 sec.
Position 3 t + 9 sec.
Position 4 t + 16 sec.
Position 5 t + 22 sec.
Position 6 t + 29 sec.
Position 7 t + 35 sec.

TABLE VII. Ceiling Heat Transfer Rate (W/m^2), Test No. 1

(Refer to Table I for Q and H.)

Position #		1	2	3	4	5	6	7
r (cm)		0	7	14	21	28	35	42
t = 1 min	ΔE	855	699	507	352	264	178	146
	q_{cond}	126	54	9	-3	-6	-6	-8
	q_{loss}	28	24	16	11	8	4	3
	q_c	1009	777	532	360	266	176	141
t = 2 min	ΔE	482	419	384	277	217	154	134
	q_{cond}	183	84	9	-2	-9	-10	-11
	q_{loss}	31	27	20	14	10	7	6
	q_c	706	530	413	289	218	151	129
t = 3 min	ΔE	316	289	255	230	171	160	126
	q_{cond}	211	93	10	0	-5	-9	-10
	q_{loss}	30	26	20	15	11	8	9
	q_c	557	408	285	245	177	159	125
t = 5 min	ΔE	226	215	193	168	139	122	103
	q_{cond}	214	104	21	4	-4	-11	-11
	q_{loss}	27	24	18	16	12	9	13
	q_c	467	343	232	188	147	120	105
t = 7 min	ΔE	174	171	170	148	129	115	92
	q_{cond}	229	106	28	6	-5	-13	-17
	q_{loss}	29	25	15	17	13	10	17
	q_c	432	302	213	171	137	112	86

TABLE VIII. Ceiling Heat Transfer Rate (W/m^2), Test No. 2

(Refer to Table I for Q and H.)

Position #		1	2	3	4	5	6	7
r (cm)		0	7	14	21	28	35	42
t = 1 min	ΔE	1316	1031	632	421	294	189	157
	q_{cond}	426	115	0	-8	-7	-7	-9
	q_{loss}	49	33	19	11	7	4	3
	q_c	1836	1179	651	424	294	186	151
t = 2 min	ΔE	815	734	550	419	275	186	157
	q_{cond}	535	169	9	-3	-10	-12	-21
	q_{loss}	51	40	26	17	11	7	6
	q_c	1401	943	585	433	296	181	142
t = 3 min	ΔE	567	584	501	355	251	187	162
	q_{cond}	534	194	18	-9	-9	-14	-37
	q_{loss}	50	42	30	20	13	9	8
	q_c	1151	820	549	366	255	182	133
t = 5 min	ΔE	409	393	377	296	220	202	144
	q_{cond}	549	214	43	0	-11	-15	-27
	q_{loss}	48	42	33	23	17	13	10
	q_c	1006	649	453	319	226	200	127
t = 7 min	ΔE	204	229	229	216	193	152	137
	q_{cond}	523	222	43	0	-17	-19	-33
	q_{loss}	43	38	31	24	17	13	11
	q_c	770	489	303	240	193	146	115

TABLE IX. Ceiling Heat Transfer Rate (W/m^2), Test No. 3

(Refer to Table I for Q and H.)

Position #		1	2	3	4	5	6	7
r (cm)		0	7	14	21	28	35	42
t = 1 min	ΔE	896	756	533	404	293	205	158
	q_{cond}	167	67	0	-3	-1	-2	-9
	q_{loss}	33	27	18	13	9	7	5
	q_c	1096	850	551	414	301	210	154
t = 2 min	ΔE	650	574	446	310	252	199	176
	q_{cond}	246	102	10	-1	-7	0	-11
	q_{loss}	37	31	22	16	12	9	7
	q_c	933	707	478	325	257	208	172
t = 3 min	ΔE	510	468	404	287	241	193	164
	q_{cond}	285	122	16	0	-9	0	-16
	q_{loss}	39	33	25	18	14	11	9
	q_c	834	623	445	305	246	204	157
t = 5 min	ΔE	281	281	293	270	211	170	146
	q_{cond}	312	132	34	0	-8	-1	-27
	q_{loss}	37	32	27	22	17	13	11
	q_c	630	445	354	292	220	182	130
t = 7 min	ΔE	117	140	140	176	140	129	129
	q_{cond}	284	123	36	15	-1	-18	-18
	q_{loss}	30	28	24	21	16	13	12
	q_c	431	291	200	212	155	124	123

TABLE X. Heat Transfer Rate to Entire Ceiling

	t =	1 min	2 min	7 min
Test No. 1	Q_c	0.178	0.145	0.090
Q = 1.17 kW H = 0.813 m	Q_c/Q	0.152	0.124	0.077
Test No. 2	Q_c	0.213	0.198	0.117
Q = 1.17 kW H = 0.584 m	Q_c/Q	0.182	0.169	0.100
Test No. 3	Q_c	0.198	0.179	0.105
Q = 1.53 kW H = 0.813 m	Q_c/Q	0.129	0.117	0.069

Q_c - total ceiling heat transfer (see p. 58).

TABLE XI. Adiabatic Ceiling Jet Temperature and Ceiling Heat Transfer Coefficient, Test No. 1

Position #		1	2	3	4	5	6	7
r (cm)		0	7	14	21	28	35	42
t = 1 min	T_{ad} *	67	59.5	58	53	45	41	38.5
	ΔT_{ad}	37.0	31.0	30.5	28.0	22.3	18.5	17.0
	h_c	27.3	25.1	17.4	12.9	11.9	9.5	8.3
t = 2 min	T_{ad}	67	59.5	58	53	45	41	38.5
	ΔT_{ad}	30.5	25.2	26.0	24.7	19.9	16.7	15.4
	h_c	23.1	21.0	15.9	11.7	11.0	9.0	8.4
t = 3 min	T_{ad}	67	59.5	58	53	45	41	38.5
	ΔT_{ad}	26.0	21.2	22.5	22.0	17.9	15.0	14.1
	h_c	21.4	19.2	12.7	11.1	9.9	10.6	8.9
t = 5 min	T_{ad}	67	59.5	58	53	45	41	38.5
	ΔT_{ad}	21.0	15.7	17.7	17.9	14.6	12.1	11.7
	h_c	22.2	21.8	13.1	10.5	10.1	9.9	9.0
t = 7 min	T_{ad}	67	59.5	58	53	45	41	38.5
	ΔT_{ad}	17.0	12.2	14.2	14.7	12.0	9.5	9.4
	h_c	25.4	24.8	12.0	11.6	11.4	11.8	9.1

Ambient Temperature = 21°C. Refer to Table I for Q and H.

* T_{ad} and ΔT_{ad} in °C; h_c in $W/m^2\ °C$.

TABLE XII. Adiabatic Ceiling Jet Temperature and Ceiling Heat Transfer Coefficient, Test No. 2

Position #		1	2	3	4	5	6	7
r (cm)		0	7	14	21	28	35	42
t = 1 min	T_{ad} *	99	81	71.5	60	53.6	46.5	43.7
	ΔT_{ad}	60.5	48.6	44.2	36.0	31.1	25.3	22.8
	h_c	30.3	24.3	14.7	11.8	9.5	7.4	6.6
t = 2 min	T_{ad}	99	81	71.5	60	53.6	46.5	43.7
	ΔT_{ad}	50.0	39.8	38.1	31.8	28.3	23.4	21.2
	h_c	28.0	23.7	15.4	13.6	10.5	7.7	6.7
t = 3 min	T_{ad}	99	81	71.5	60	53.6	46.5	43.7
	ΔT_{ad}	43.3	33.2	32.8	28.0	25.7	21.5	19.5
	h_c	26.6	24.7	16.7	13.1	9.9	8.5	6.8
t = 5 min	T_{ad}	99	81	71.5	60	53.6	46.5	43.7
	ΔT_{ad}	33.0	23.2	24.0	21.4	20.9	17.7	16.5
	h_c	30.5	28.0	18.9	14.9	10.8	11.3	7.7
t = 7 min	T_{ad}	99	81	71.5	60	53.6	46.5	43.7
	ΔT_{ad}	27.2	17.1	18.3	16.3	16.9	14.3	13.5
	h_c	28.3	28.6	16.6	14.7	11.4	10.2	8.5

Ambient Temperature = 19.3 °C. Refer to Table I for Q and H .

*T_{ad} and ΔT_{ad} in °C; h_c in W/m^2 °C .

TABLE XIII. Adiabatic Ceiling Jet Temperature and Ceiling Heat Transfer Coefficient, Test No. 3

Position #		1	2	3	4	5	6	7
r (cm)		0	7	14	21	28	35	42
t = 1 min	T_{ad} *	70	64	58	52	47	43.5	42
	ΔT_{ad}	33.1	33.3	33.2	32.7	30.7	29.2	27.8
	h_c	33.1	25.5	16.6	12.7	9.8	7.2	5.5
t = 2 min	T_{ad}	70	64	58	52	47	43.5	42
	ΔT_{ad}	26.7	27.7	28.7	29.0	27.8	27.0	26.1
	h_c	34.9	25.5	16.7	11.2	9.2	7.7	6.6
t = 3 min	T_{ad}	70	64	58	52	47	43.5	42
	ΔT_{ad}	22.1	23.3	25.0	26.0	25.1	24.9	24.2
	h_c	37.7	26.7	17.8	11.7	9.8	8.2	6.5
t = 5 min	T_{ad}	70	64	58	52	47	43.5	42
	ΔT_{ad}	15.6	17.2	19.1	21.0	20.7	21.2	20.9
	h_c	40.4	25.9	18.5	13.9	10.6	8.6	6.2
t = 7 min	T_{ad}	70	64	58	52	47	43.5	42
	ΔT_{ad}	11.2	12.7	14.6	16.7	17.0	17.9	17.9
	h_c	38.5	22.9	13.7	12.7	9.1	6.9	6.9

Ambient Temperature = 18 °C. Refer to Table I for Q and H.

* T_{ad} and ΔT_{ad} in °C; h_c in $W/m^2\ ^oC$.

TABLE XIV. Dimensionless Ceiling Heat Transfer Coefficient (h'_c)

Test No. 1

Position #		1	2	3	4	5	6	7
r (cm)		0	7	14	21	28	35	42
r/H		0	0.086	0.172	0.258	0.344	0.431	0.517
	t (min)							
	1	0.067	0.062	0.043	0.032	0.029	0.023	0.020
	2	0.057	0.052	0.039	0.029	0.027	0.022	0.021
h'_c	3	0.053	0.047	0.031	0.027	0.024	0.026	0.022
	5	0.055	0.054	0.032	0.026	0.025	0.024	0.022
	7	0.063	0.061	0.030	0.029	0.028	0.029	0.022

Refer to Table I for Q and H .

$$h'_c = \frac{h_c}{\rho_\infty C_p \sqrt{gH}\,(Q^*)^{1/3}} \qquad Q^* = \frac{Q}{\rho_\infty C_p T_\infty \sqrt{gH}\,H^2}$$

TABLE XV. Dimensionless Ceiling Heat Transfer Coefficient (h'_c)

Test No. 2

Position #		1	2	3	4	5	6	7
r (cm)		0	7	14	21	28	35	42
r/H		0	0.120	0.240	0.360	0.479	0.599	0.719
	t (min)							
	1	0.067	0.054	0.033	0.026	0.021	0.016	0.015
	2	0.062	0.053	0.034	0.030	0.023	0.017	0.015
h'_c	3	0.059	0.055	0.037	0.029	0.022	0.019	0.015
	5	0.058	0.062	0.042	0.033	0.024	0.025	0.017
	7	0.063	0.063	0.037	0.033	0.025	0.023	0.019

Refer to Table I for Q and H .

$$h'_c = \frac{h_c}{\rho_\infty C_p \sqrt{gH}\,(Q^*)^{1/3}} \qquad Q^* = \frac{Q}{\rho_\infty C_p T_\infty \sqrt{gH}\,H^2}$$

TABLE XVI. Dimensionless Ceiling Heat Transfer Coefficient (h'_c)

Test No. 3

Position #		1	2	3	4	5	6	7
r (cm)		0	7	14	21	28	35	42
r/H		0	0.086	0.172	0.258	0.344	0.431	0.517
	t (min)							
	1	0.075	0.058	0.037	0.029	0.022	0.016	0.012
	2	0.079	0.058	0.038	0.025	0.021	0.017	0.015
h'_c	3	0.085	0.060	0.040	0.026	0.022	0.019	0.015
	5	0.091	0.058	0.042	0.031	0.024	0.019	0.014
	7	0.087	0.052	0.031	0.029	0.021	0.016	0.016

Refer to Table I for Q and H .

$$h'_c = \frac{h_c}{\rho_\infty C_p \sqrt{gH}\,(Q^*)^{1/3}} \qquad Q^* = \frac{Q}{\rho_\infty C_p T_\infty \sqrt{gH}\,H^2}$$

TABLE XVII. Comparison between Parameters for Experimental Case (Small Scale Fire) and Prediction for a "Real Room Fire."

Type of Ceiling	Q (kW)	H (m)	Q^*	$\left(h'_c\right)_{r=0}$	ΔT_{ad} $r=0$ (^oC)	q_c $r=0$ $t=0$ (W/m^2)	t_c (sec)
1/16" steel	1.17	.584	.00413	$\frac{h_c}{450.6}$	76°C	2000	162
1/2" plaster-board	200	1.825	.041	$\frac{h_c}{1719.1}$	347°C	41,600	109

See discussion, page 64.

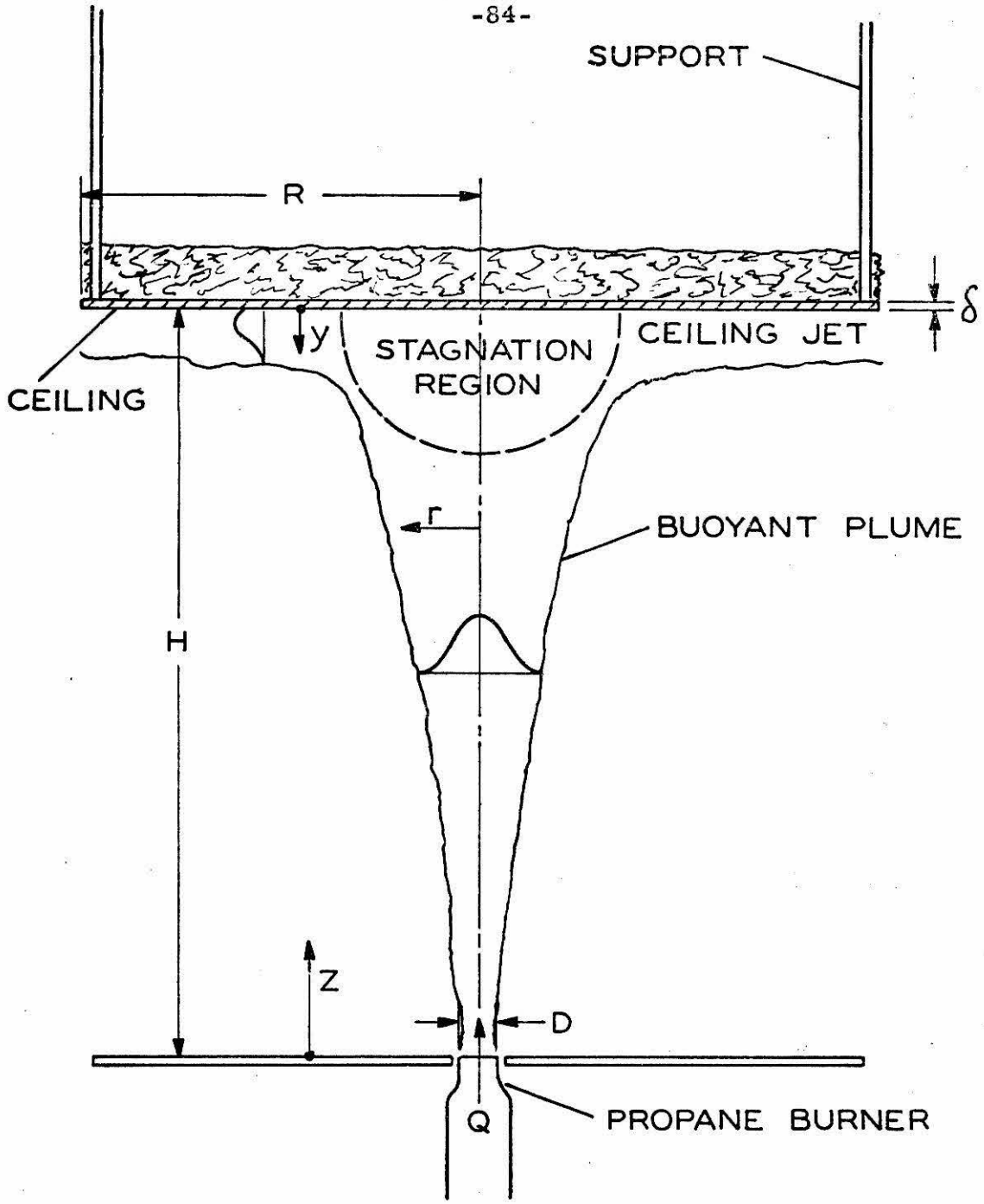

FIG. 1 DIAGRAM OF EXPERIMENTAL MODEL

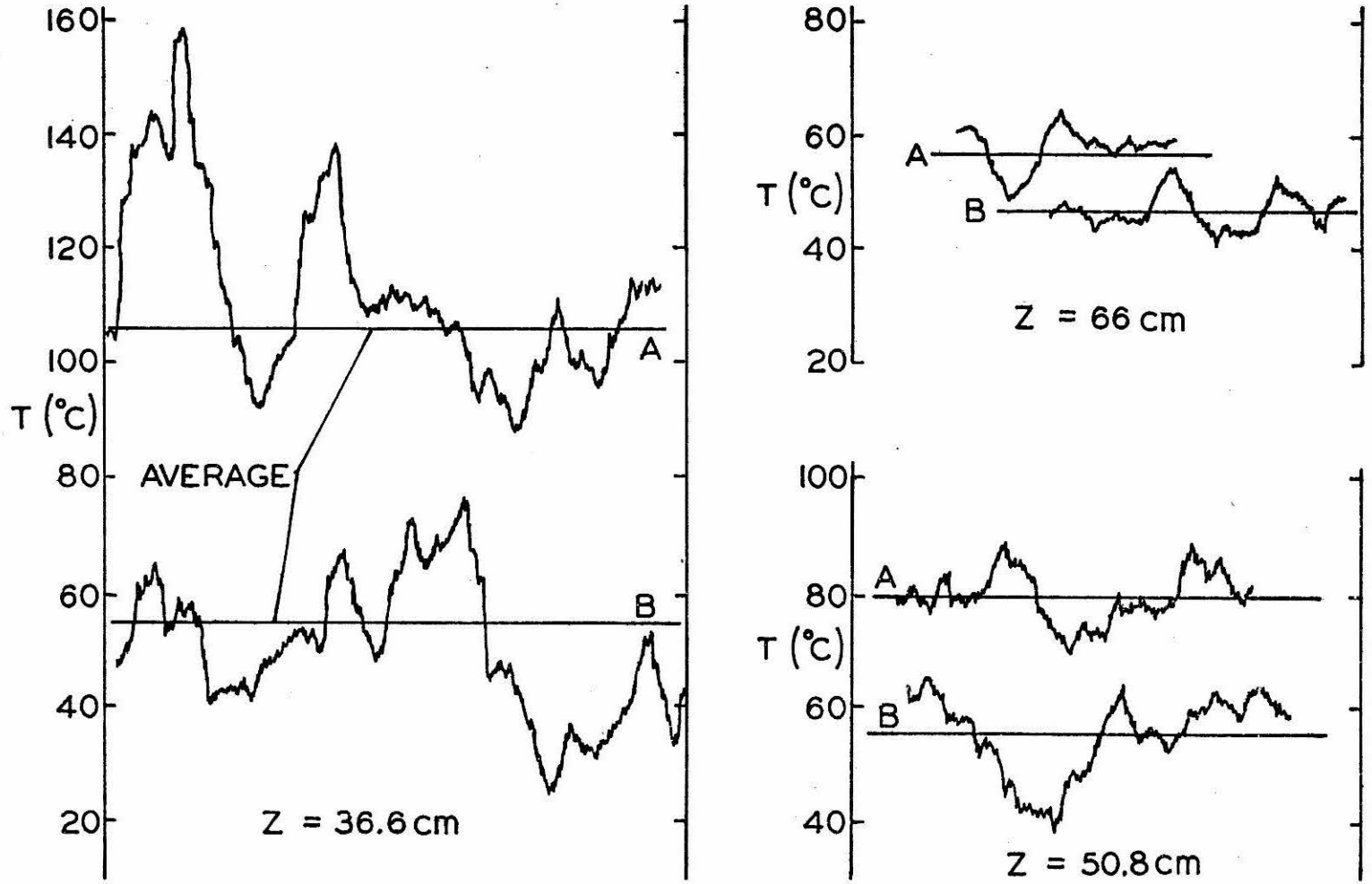

A CENTRELINE TEMPERATURE
B TEMP. AT POSITION OF MAXIMUM SLOPE OF TEMP. PROFILE

FIG. 2. RECORDED PLUME TEMPERATURES

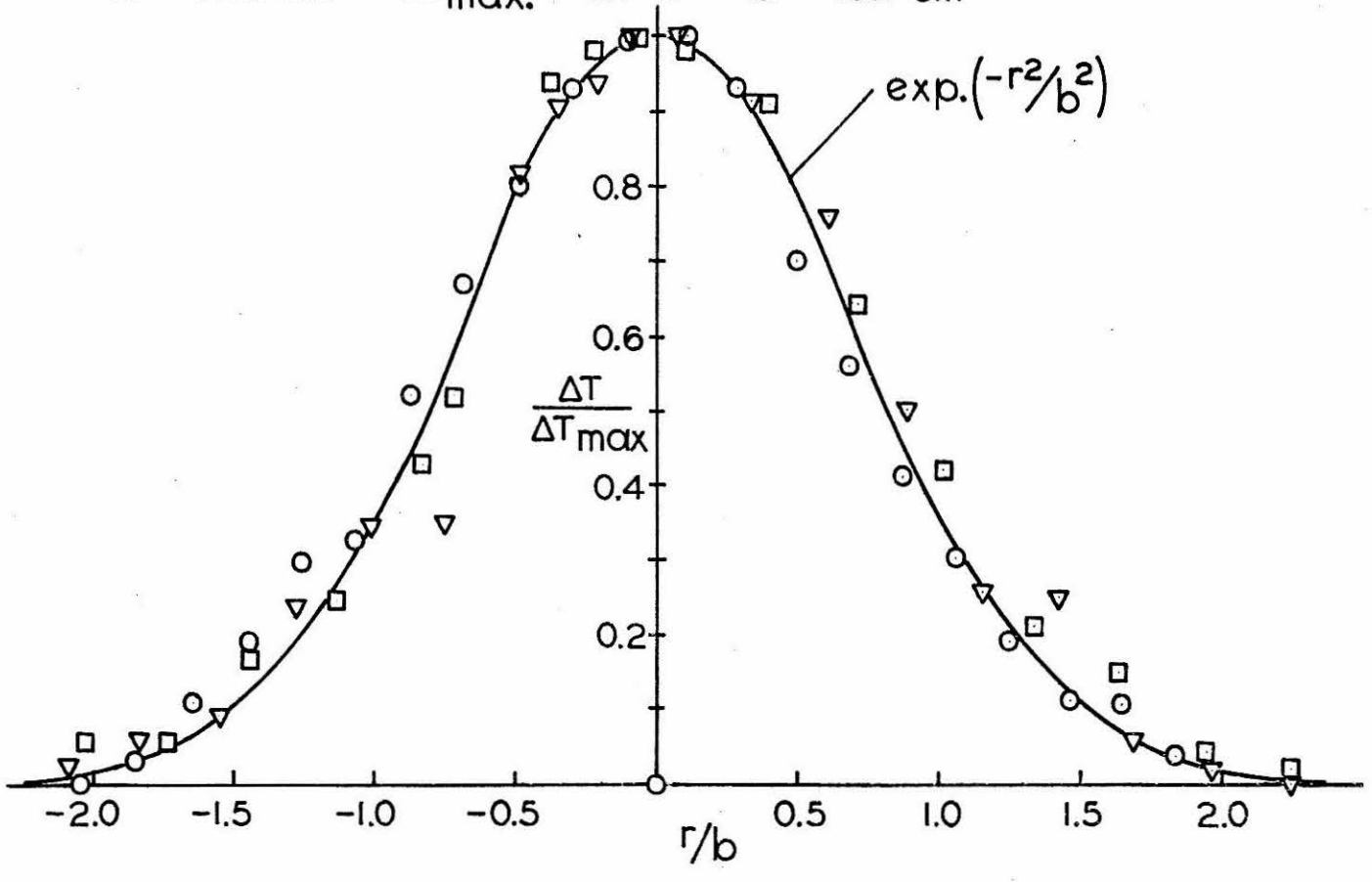

FIG. 3 NORMALIZED CROSS-SECTIONAL PLUME TEMPERATURES

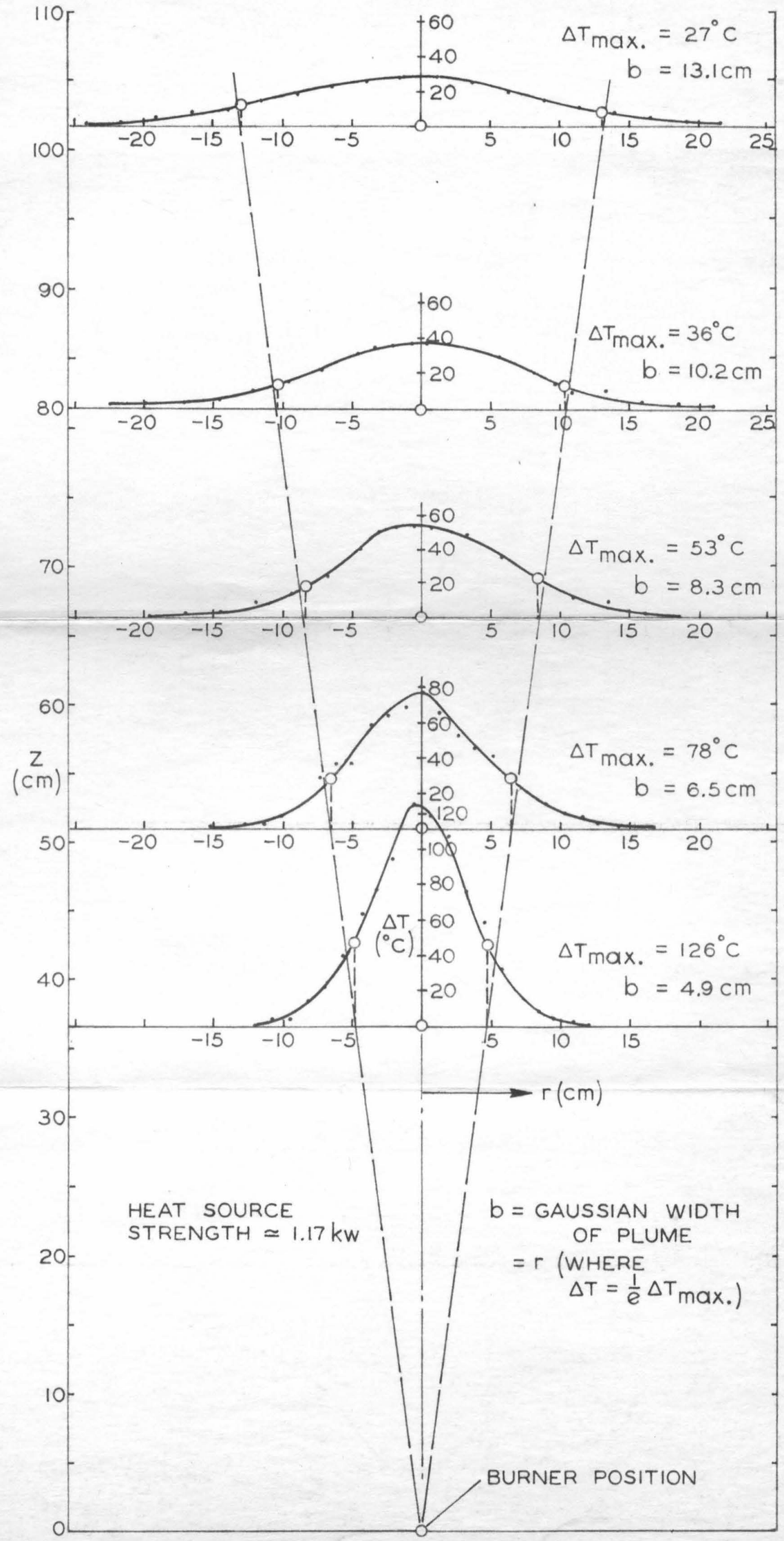

FIG. 4 BUOYANT PLUME TEMPERATURE DISTRIBUTION

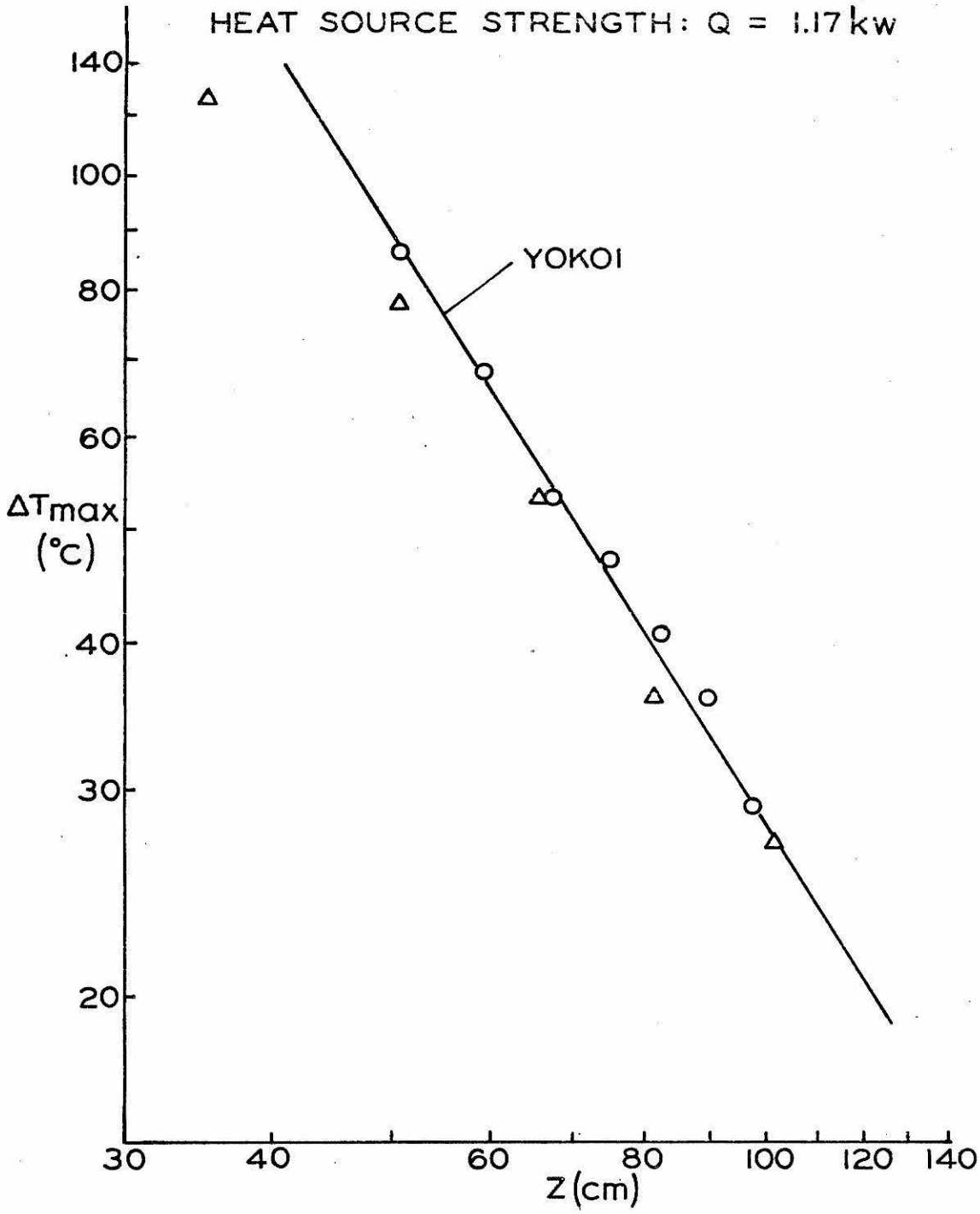

FIG. 5 BUOYANT PLUME CENTRELINE TEMPERATURE VARIATION

⊡	r = 0.178m,	Q ≃ 1.17 kw,	$\Delta T_{max.}$ = 37°C,	b = 3.94 cm
△	0.254	1.17	30	3.56
X	0.381	1.17	22	4.09
▽	0.254	1.53	40	3.56
⊙	0.381	1.53	27	4.83

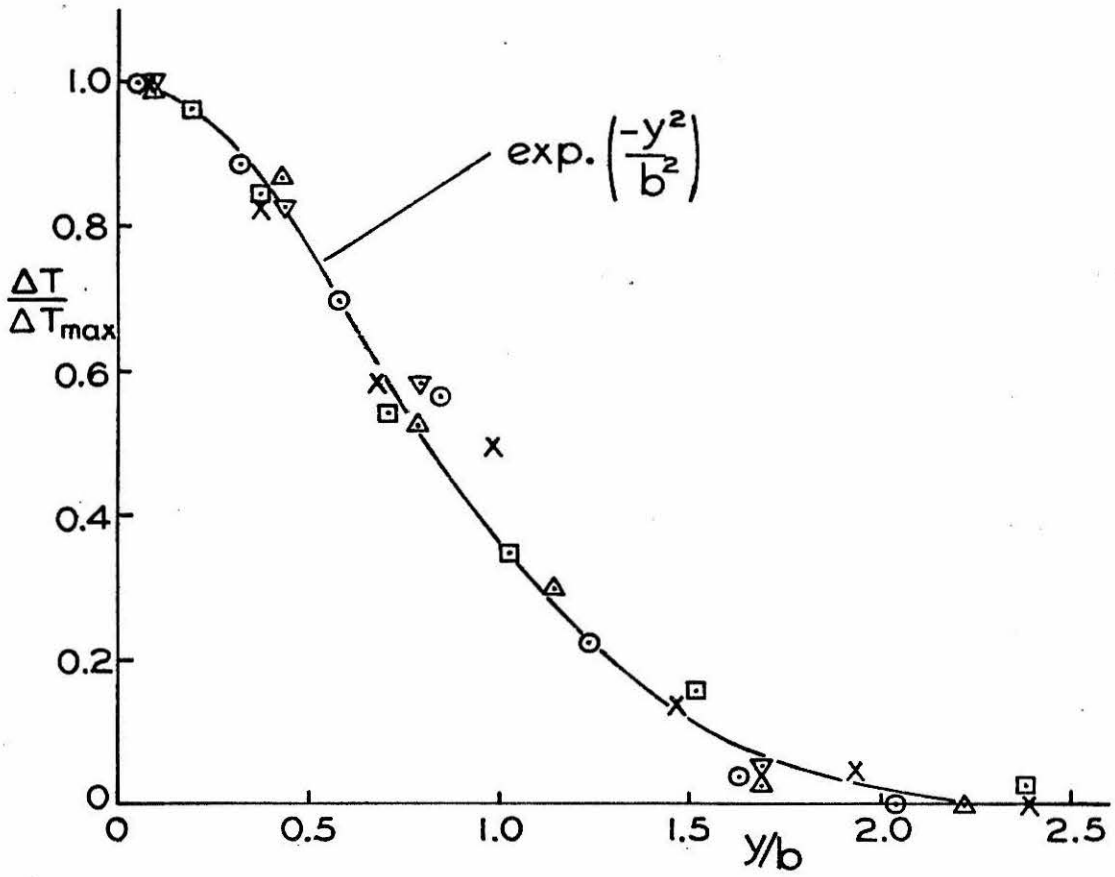

FIG. 6 CEILING JET VERTICAL TEMP. DISTRIBUTION (H = 0.813 m)

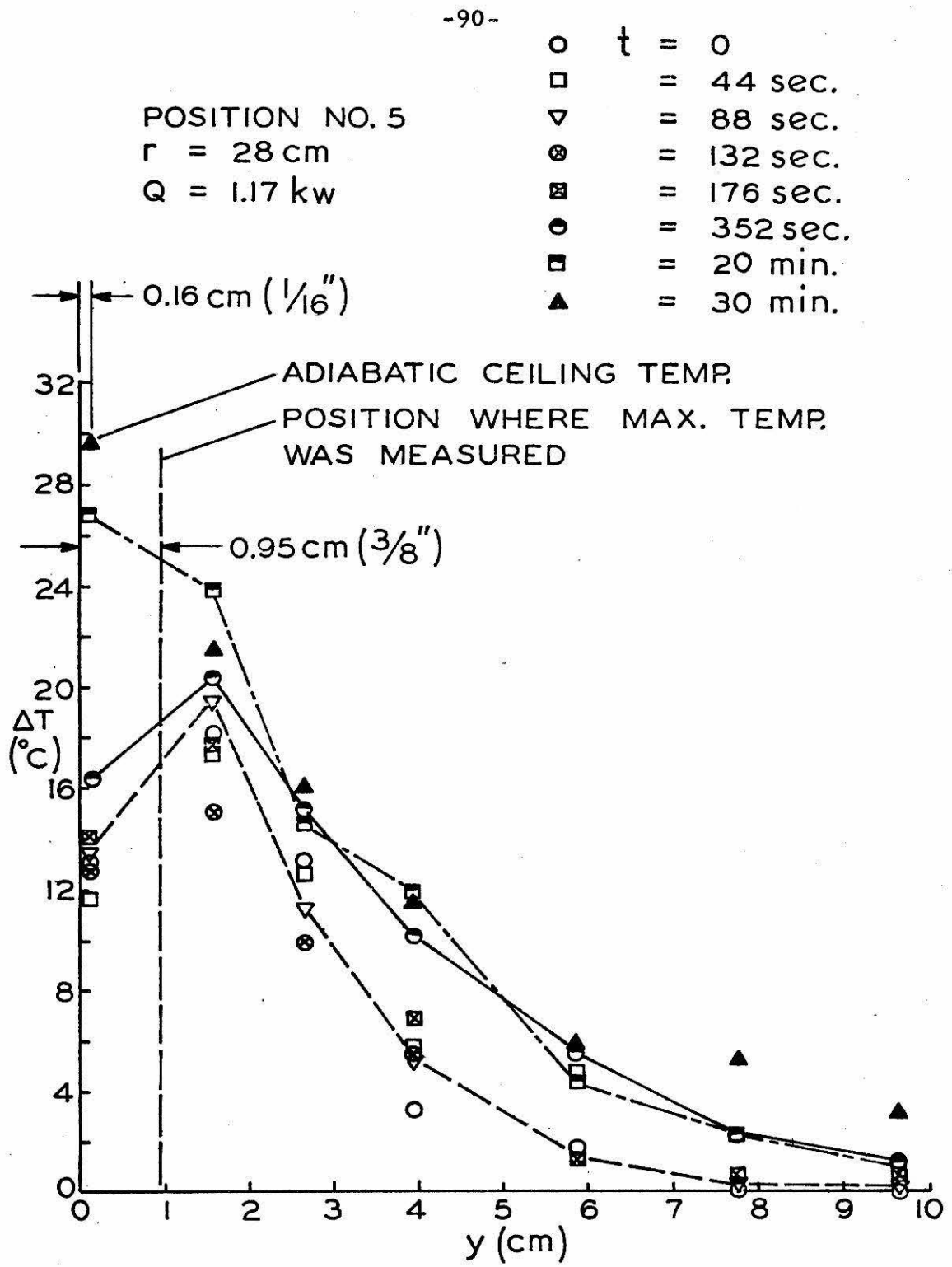

FIG. 7 VARIATION IN CEILING JET TEMPERATURE PROFILES WITH TIME

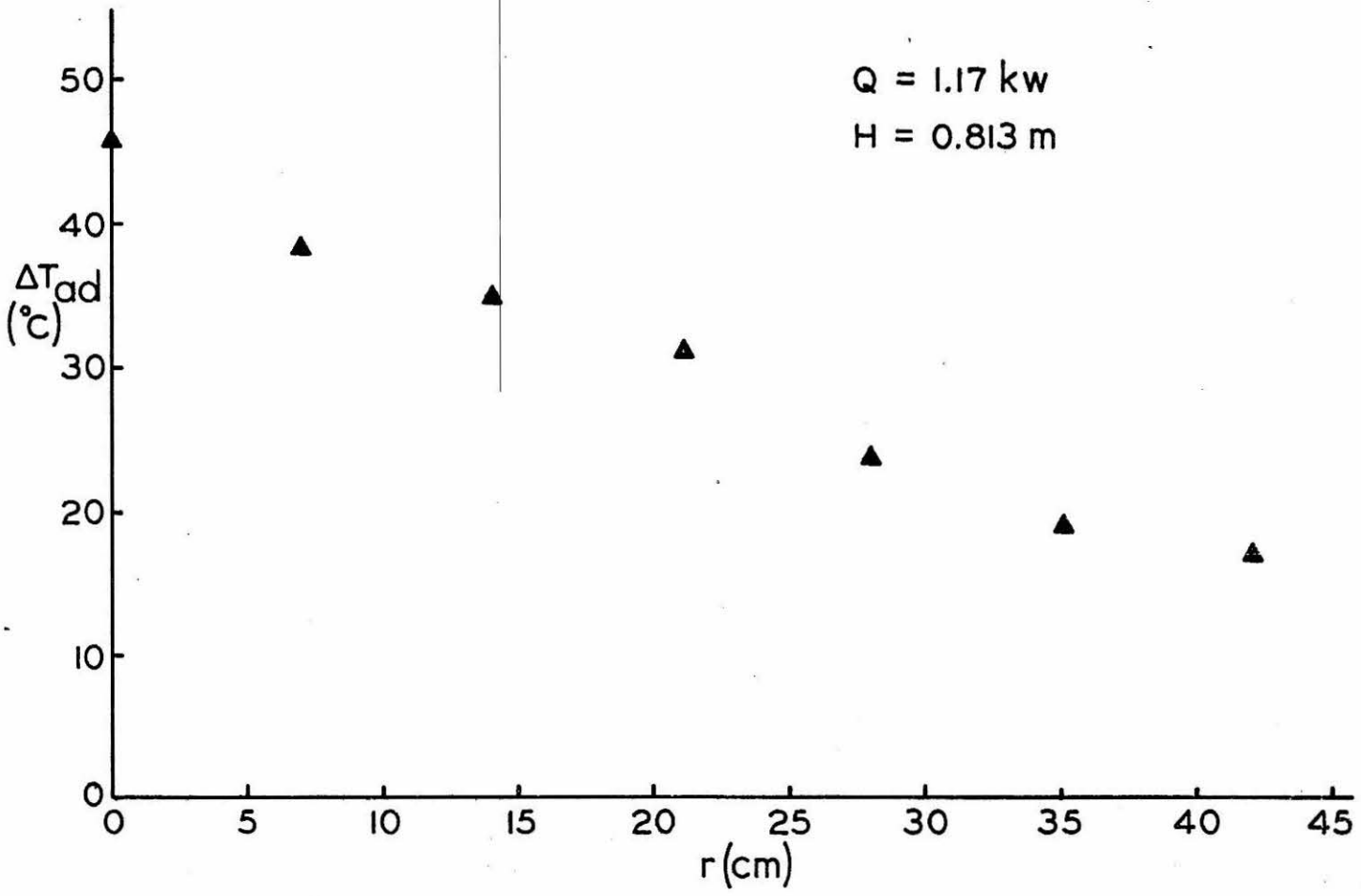

FIG. 8 ADIABATIC CEILING JET TEMPERATURE VARIATION

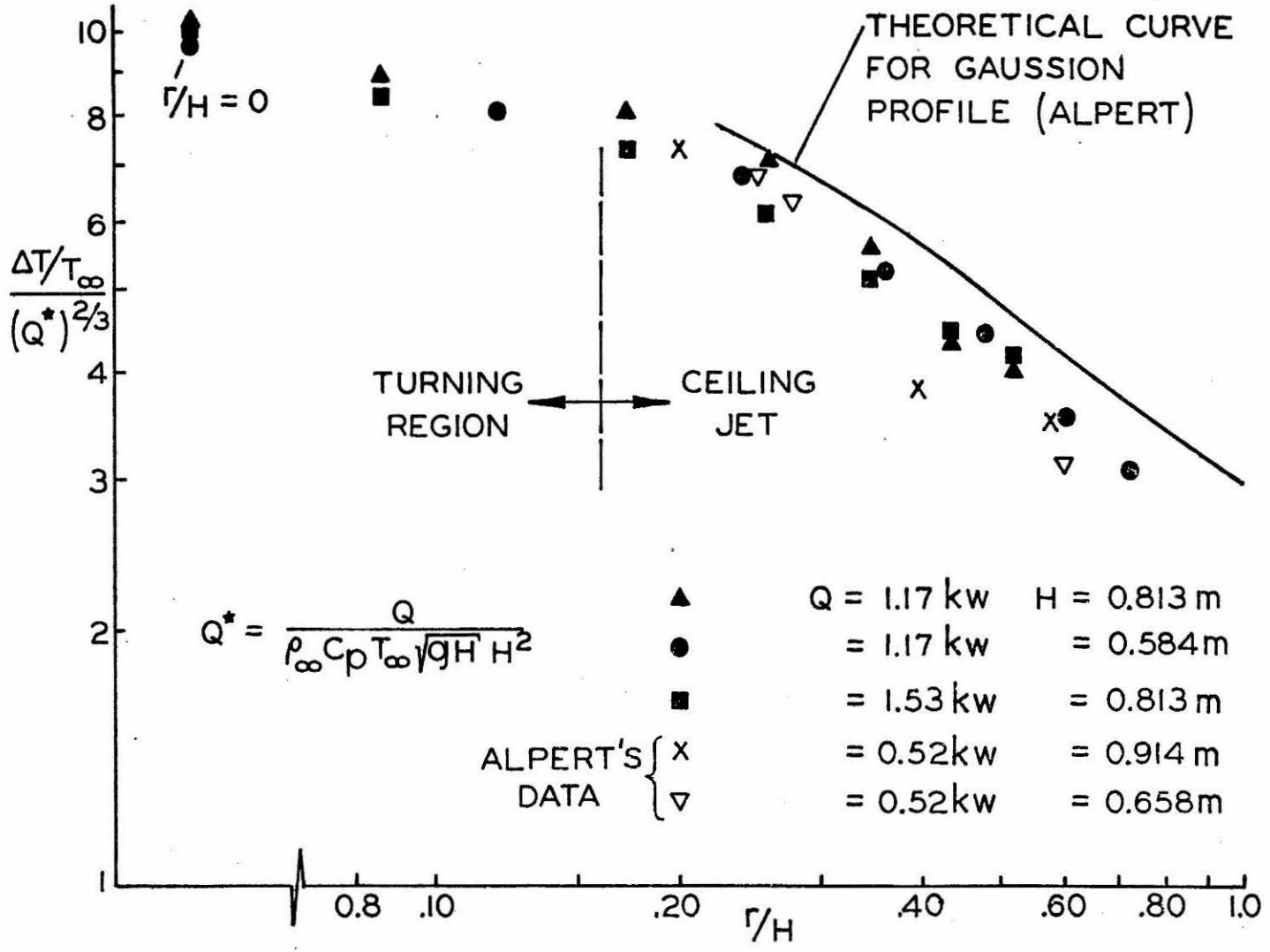

FIG. 9 DIMENSIONLESS ADIABATIC CEILING JET TEMPERATURE

	Q^* (10^{-3})	REFERENCE
——— ΔT_{ad} – – – $1/\sqrt{2}\ \Delta T_{ad}$	1.8 – 4.13	AUTHOR
o	0.019 – 0.47	MILLER [11]
●	5.4	THOMPSON [12]
■	14.4	"
◆	28.9	"
▲	54.2	"

$$Q^* = \frac{Q}{\rho_\infty C_p T_\infty \sqrt{gH}\, H^2}$$

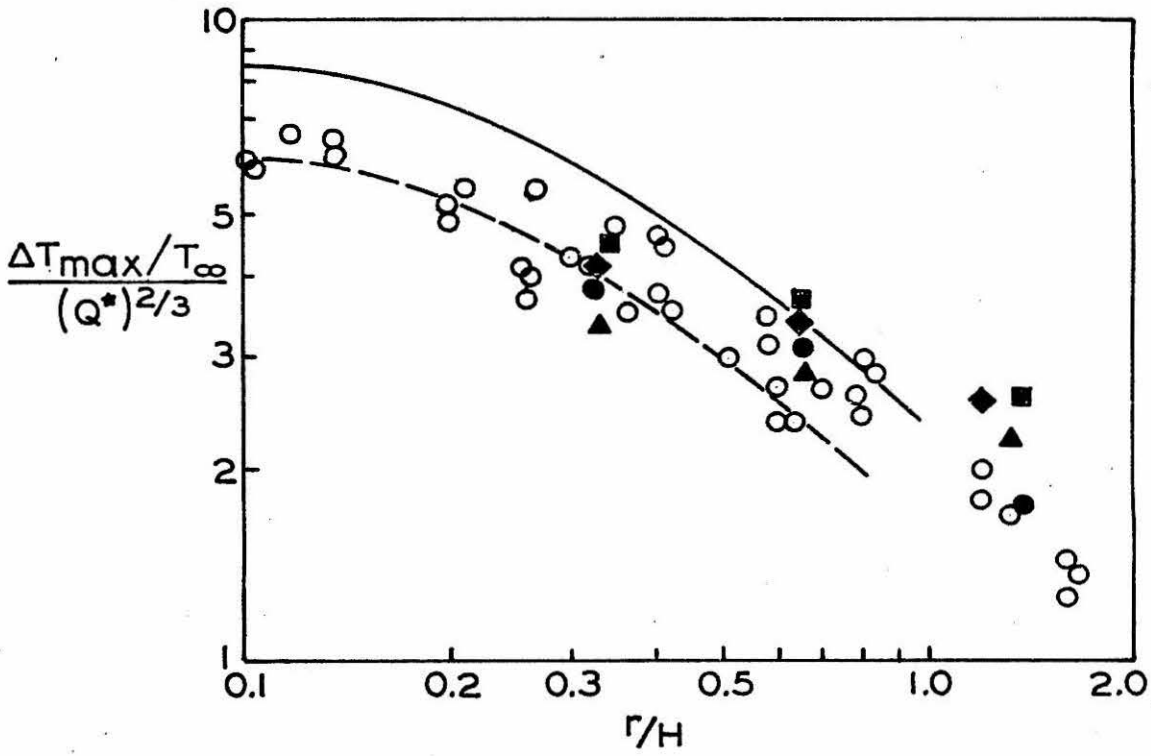

FIG. 10 DIMENSIONLESS ADIABATIC CEILING JET TEMPERATURE: COMPARISON BETWEEN SMALL & LARGE SCALE EXPERIMENTS

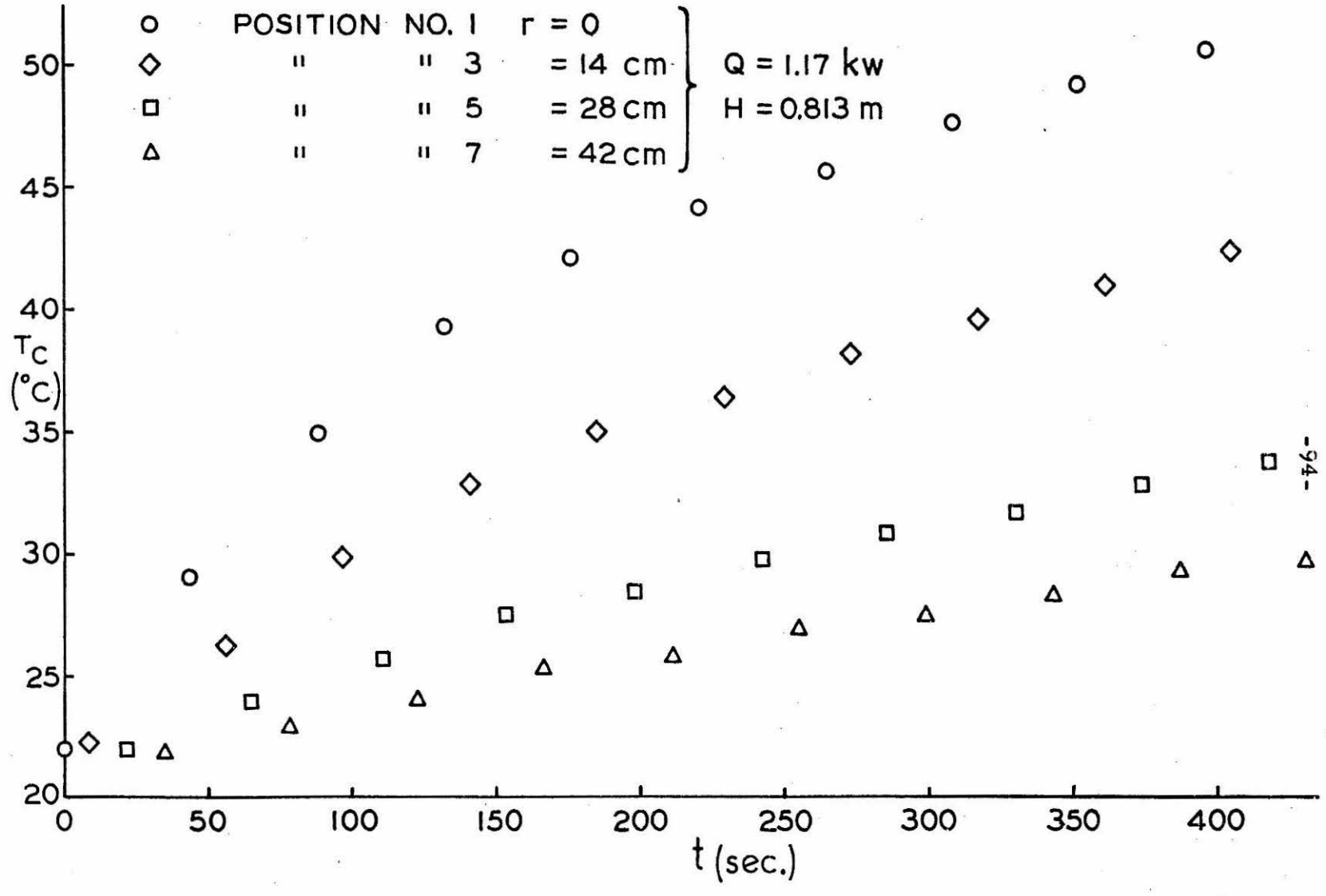

FIG. 11 CEILING TEMPERATURE INCREASE WITH TIME

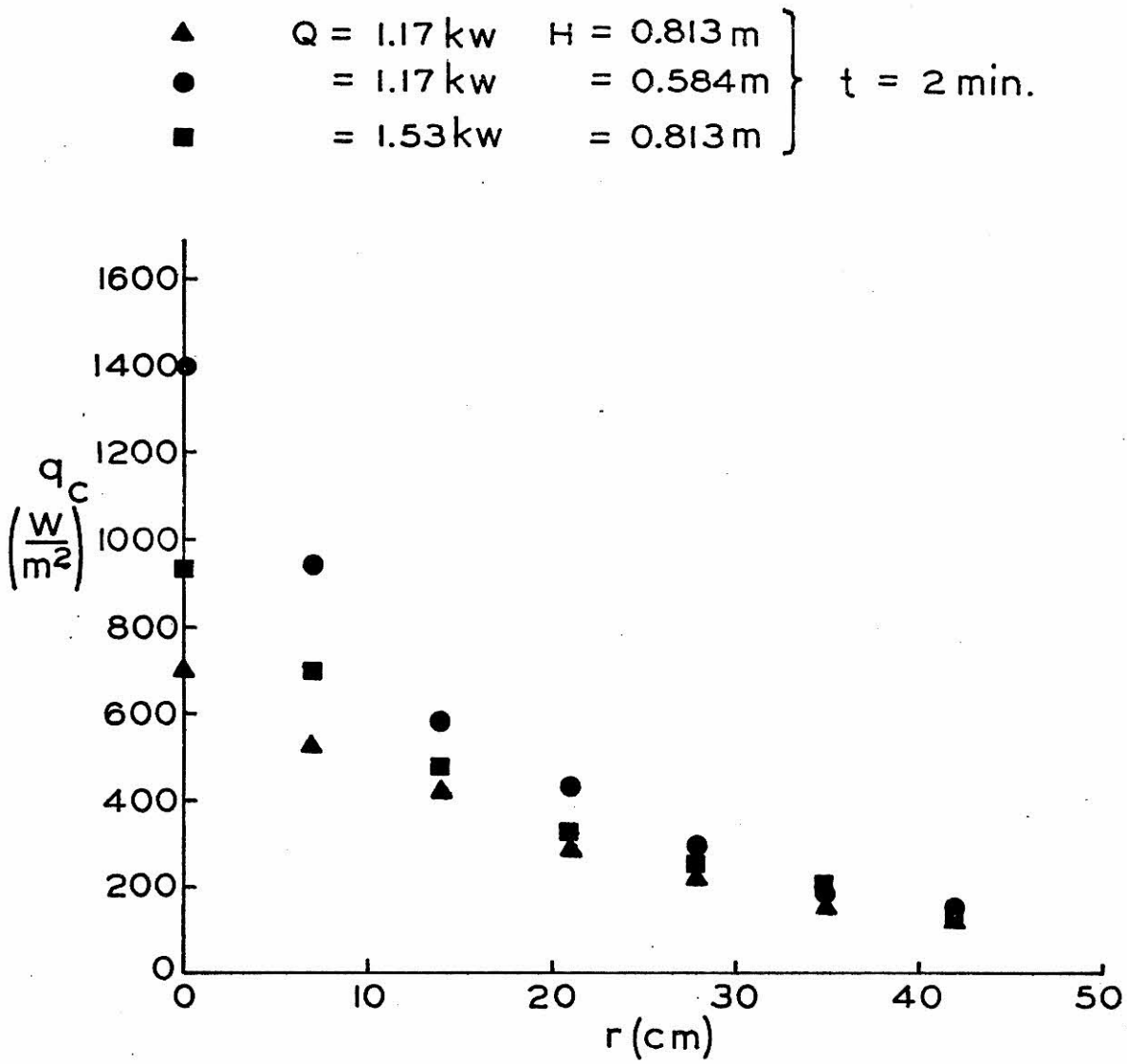

FIG. 12 RADIAL VARIATION OF CEILING HEAT TRANSFER

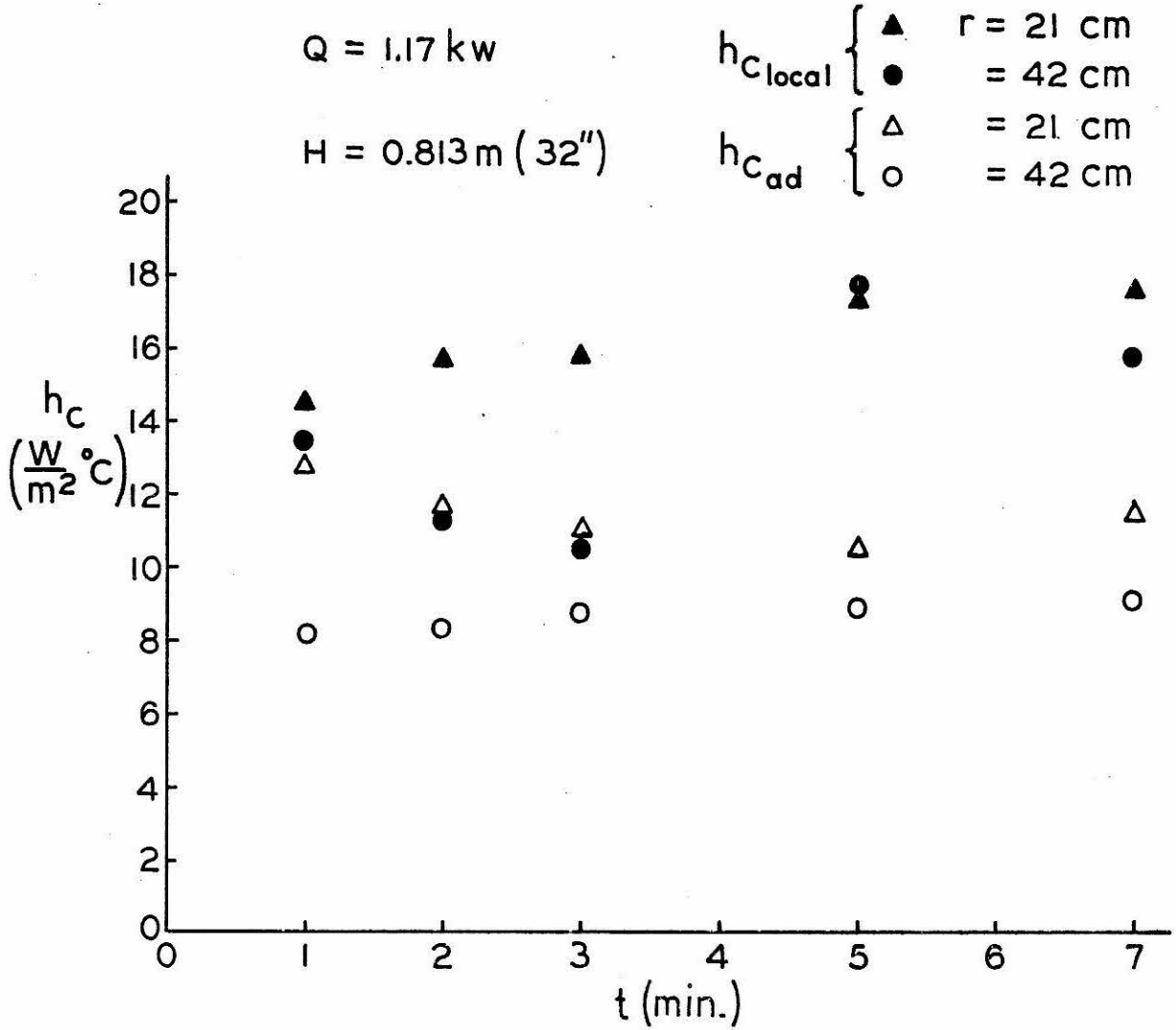

FIG. 13 COMPARISON BETWEEN $h_{c_{local}}$ AND $h_{c_{ad}}$

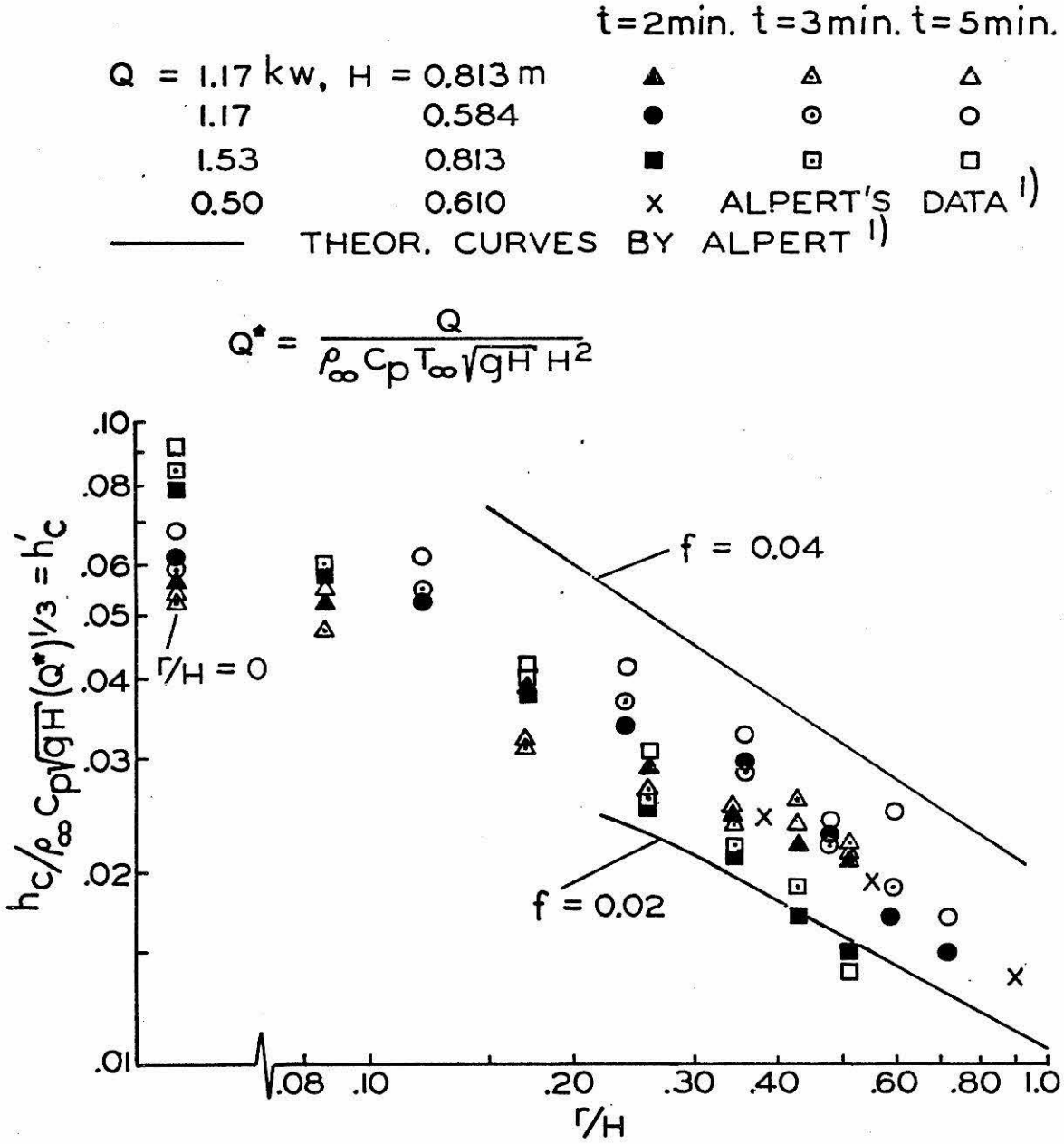

FIG. 14 DIMENSIONLESS CEILING HEAT TRANSFER COEFFICIENT

APPENDIX A

Calculation of Strength of Heat Source

The strength of the heat source can be calculated from the measured flow rates of gas and air, and from the heating value of propane, assuming full reaction. The amount of air that has to be supplied in order to ensure stoichiometric burning can be calculated from the following reaction equation:

$$C_3H_8 + 5O_2 + 5(79/21)N_2$$

propane air

$$\rightarrow 3CO_2 + 4H_2O + 5(79/21)N_2 \quad . \qquad \text{(A-1)}$$

Hence, five moles of oxygen (i.e., 5 moles of air) are needed for every one mole of propane.

Based on mole masses:

C_3H_8	:	$5O_2 + 5(79/21)N_2$	
$3(12) + 8$	:	$5(32) + 5(79/21)(28)$	
$= 36 + 8$	:	$= 160 + 526.6$	
$= 44$	:	$= 686.7$	(A-2)

Now, assuming that the gas and air are mixed at the same temperature (ambient temperature), then

$$\rho_{air} = 1.18 \text{ kg/m}^3 = 1.18 \times 10^{-3} \text{ g/cc}$$

$$\rho_{propane} = 1.87 \text{ kg/m}^3 = 1.87 \times 10^{-3} \text{ g/cc}$$

$\therefore$ stoichiometric air/fuel ratio:

$$(a/f)_{\substack{\text{stoich.} \\ \text{volumetric}}} = \frac{44/1.87}{686.7/1.18} = 0.0404$$

or $$(f/a)_s = 24.7 \quad .$$

Assume a heat source strength of 1 kW is required: in Chemical Engineers' Handbook[13] the heat of combustion of propane (for combustion at atmospheric pressure and 20°C) is given as

$$\dot{Q}_c = 526.3 \frac{\text{kg cal}}{\text{gm mole}} = \frac{526.3}{44} \frac{\text{cal}}{\text{mole}} \cdot \frac{\text{mole}}{\text{gm}}$$

$$= 11961 \frac{\text{cal}}{\text{gm}} = 50080 \text{ kJ/kg} \quad (\equiv 21530 \text{ Btu/lb}) \ .$$

Hence, the required flowrate of propane is

$$\dot{m}_{\text{propane}} = \frac{1}{50.08} = 0.02 \text{ gm/s} \ .$$

∴ Required volumetric flowrate of propane

$$= \frac{0.02}{1.87 \times 10^{-3}} = 10.7 \text{ cc/s} \ .$$

Required air flow

$$= 10.7 \times 24.7 = 264 \text{ cc/s} \ .$$

∴ Total volumetric flow rate of fuel

$$= 274.7 \text{ cc/s} \ .$$

Now consider a gas burner with 2.54 cm (1") diameter nozzle exit:

$$A_e = \frac{\pi}{4} (2.54)^2 = 5.07 \text{ cm}^2 \ .$$

∴ Exit velocity

$$u_e = \frac{274.7}{5.07} = 54.2 \text{ cm/s} \qquad (\simeq 1.78 \text{ ft/s})$$

Hence, the required heat input results in a nozzle exit velocity $u_e = 54.2$ cm/s, which is greater than the flame velocity of propane ($\simeq 45$ cm/s).

Assuming that the stainless steel grid covers a maximum of 30 per cent of the nozzle exit area, then

$$u_e \simeq 1.3 \times 54.2 = 70.5 \text{ cm/s} \ .$$

APPENDIX B

Calculation of Specific Heat of Insulation

The insulating material used was Owen-Corning R11 Fiberglas Wool, with a thickness of $3\frac{1}{2}$" (9 cm). Now

$$\text{R-value} = \frac{\text{thickness(uncompressed)}}{\text{conductivity}} \quad \left(\frac{\text{Btu - inch}}{\text{hr ft}^2\ ^\circ\text{F}}\right)$$

(specified at 75°F mean)

accuracy ± 10 per cent

$$\therefore\ k_{R11} = \frac{3.5}{11} = 0.318\ \frac{\text{Btu - inch}}{\text{hr ft}^2\ ^\circ\text{F}} = 0.045\ \text{W/m}\ ^\circ\text{C}\ .$$

Uncompressed density:

$$\rho_{R11} = 0.65\ \text{lb/ft}^3 = 10.41\ \text{kg/m}^3\ .$$

The specific heat of R11 can now be calculated by calculating the weight ratio of glass and air, and combining their specific heats.

The following values are obtained from Eckert and Drake[8]:

$$\rho_{glass} \approx 160\ \text{lb/ft}^3 = 2560\ \text{kg/m}^3\ ,$$

$$C_{p_{glass}} = 0.8 \times 10^3\ \text{J/kg}\ ^\circ\text{K}\ ,$$

$$\rho_{\substack{air \\ 40^\circ C}} \simeq 1.15\ \text{kg/m}^3$$

$$C_{p_{air}} = 1.006 \times 10^3\ \text{J/kg}\ ^\circ\text{K}\ .$$

Hence, volume of glass/m^3 of R11

$$= \frac{10.41}{2560} = 4.1 \times 10^{-3}\ \text{m}^3\ .$$

Now consider the following energy balance:

$$C_{p_{R11}} \rho_{R11} V \Delta T = C_{p_{air}} (1 - 4.1 \times 10^{-3}) V \rho_{air} \Delta T + C_{p_{glass}} \cdot 4.1 \times 10^{-3} \rho_{glass} \Delta T \qquad \text{(B-1)}$$

$$\therefore C_{p_{R11}} = \frac{0.9959\, C_{p_{air}} \rho_{air} + .0041\, C_{p_{glass}} \rho_{glass}}{\rho_{R11}}$$

$$= 0.954 \times 10^{3} \text{ J/kg } ^{o}\text{K} .$$

$$\therefore \nu_{R11} = \frac{k}{\rho C_p} = \frac{0.046}{10.41 \times 0.954 \times 10^{3}} = 4.6 \times 10^{-6} \text{ m}^2/\text{s} .$$

APPENDIX C

Effect of Thermocouple Wire on Local Temperature Measurement on Ceiling

The effect of the conduction along a single thermocouple lead on the local temperature and $\partial T/\partial t$ measurement was analyzed by McMahon[14]. He considered a thermocouple wire (2) perpendicular to a thin sheet (1) (refer to sketch below). The region (3) was considered separately since this simplified the writing of boundary conditions for the other two regions.

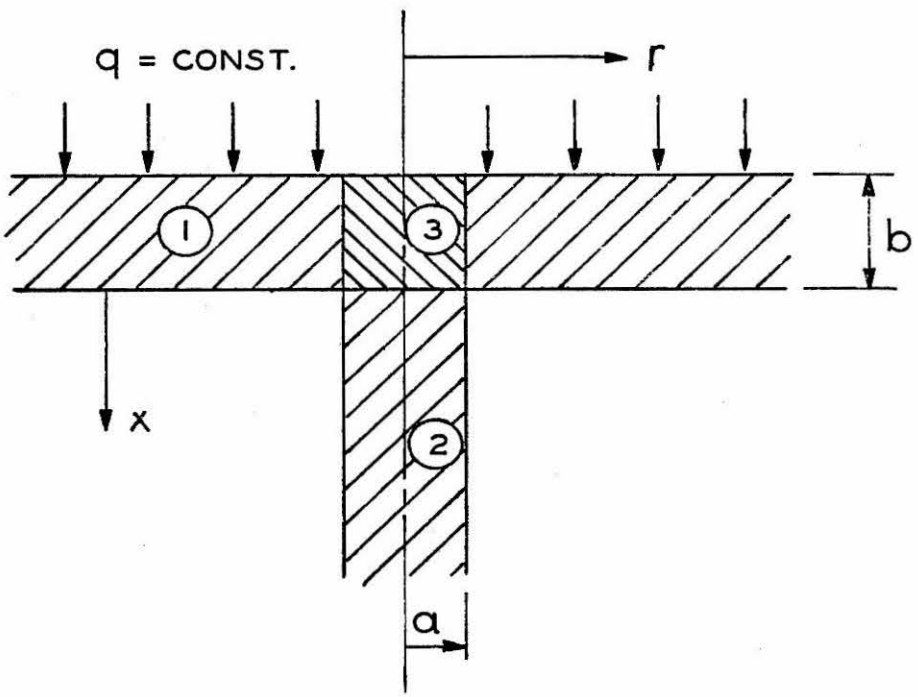

The following assumptions were made: (i) $T(r = a, t) = T(x = 0, t)$, i.e., the region (3) has an infinite conductivity but a finite heat capacity, so that the storage term for this region will be included; (ii) no temperature gradients exist through sheet (1) normal to the sur-

face; (iii) no heat loss from the underside of the sheet nor from the wire surface.

The heat equation in polar coordinates for region (1) is:

$$\rho_1 C_1 \frac{\partial T_1}{\partial t} = \frac{q}{b} + \frac{k_1}{r} \frac{\partial}{\partial r}\left(r \frac{\partial T_1}{\partial r} \right) \qquad (C-1)$$

with initial and boundary conditions:

$$\begin{aligned} T_1(r, 0) &= 0 \\ T_1(r \to \infty, t) &= \text{finite} \\ T_1(a, t) &= F(t) \end{aligned} \qquad (C-2)$$

where $F(t)$ is determined later from the heat balance for region (3).

For region (2):

$$\rho_2 C_2 \frac{\partial T_2}{\partial x} = k_2 \frac{\partial^2 T}{\partial x^2} \qquad (C-3)$$

with initial and boundary conditions:

$$\begin{aligned} T_2(x, 0) &= 0 \\ T_2(x \to \infty, t) &= \text{finite} \\ T_2(0, t) &= F(t) \end{aligned} \qquad (C-4)$$

Letting $T_3 = F(t)$, the heat balance for region (3) is:

$$\frac{\partial F}{\partial t} = \frac{q}{\rho_3 C_3 b} + \frac{2 k_1}{\rho_3 C_3 a} \frac{\partial T_1(a, t)}{\partial r} + \frac{k_2}{\rho_3 C_3 b} \frac{\partial T_2(0, t)}{\partial x} . \qquad (C-5)$$

These equations are then solved and combined for the given initial and boundary conditions.

Finally, the following expression for the measured temperature $T_3 = F(t)$ is obtained:

$$F(t) = \frac{q}{\rho_3 C_3 b}\left[t + \frac{a^2 \sqrt{\kappa_2}}{4 \kappa_1 b} \frac{\rho_2 C_2}{\rho_3 C_3} t^{\frac{1}{2}} \left\{ \frac{\Gamma'(3/2)}{\Gamma(3/2)} - \frac{2}{\sqrt{\pi}} \log \frac{\kappa_1 t}{a^2} \right\} \right] \qquad (C-6)$$

$$\kappa \equiv k / \rho C$$

which is of the form

$$F(t) = \frac{q}{\rho_3 C_3 b}(t + \varepsilon) \qquad (C-7)$$

where $F(t) = \frac{q}{\rho_3 C_3 b}\, t = T_3$ would be the temperature expected without the presence of the wire, i.e.,

$$q = \rho_3 C_3 b \frac{\partial T_3}{\partial t} \quad . \qquad (C-8)$$

Hence, calculating the second term in the square brackets of (C-6) will yield the error involved in measuring the sheet temperature.

To get an idea of the magnitude of this error ε, consider the case where the plate and wire are of the same material (sheet steel in this case). Then

$$\varepsilon = \frac{a^2}{4\sqrt{\varkappa_1}\, b}\, t^{\frac{1}{2}} \left\{ \frac{\Gamma'(3/2)}{\Gamma(3/2)\Gamma(3/2)} - \frac{2}{\sqrt{\pi}} \log \frac{\varkappa_1 t}{a^2} \right\} \quad . \qquad (C-9)$$

Using values for low carbon steel from Eckert and Drake[8]:

$$\varkappa_2 = \varkappa_1 = 1.172 \times 10^{-5}\ m^2/s \quad .$$

For 0.005" thermocouple leads and a 1/16" ceiling:

$$a = 0.0025" = 6.35 \times 10^{-5}\ m$$

$$\therefore \quad a^2 = 40.32 \times 10^{-10}\ m^2$$

$$b = 1/16" = 1.58 \times 10^{-3}\ m \quad .$$

Let t = 120 sec. Then

$$\varepsilon \simeq -546.4 \times 10^{-4} \quad .$$

$$\therefore \quad F(t) \simeq \text{const.}\,[120 - 0.0546]$$

$$= \text{const.}\,[1 - 4.5 \times 10^{-4}] \quad .$$

This shows that the error is much less than one per cent.

For t = 420 sec. (7 min.),

$$\varepsilon \simeq -603.9 \times 10^{-4}$$

$$\therefore \quad F(t) \simeq \text{const.}\,[1 - 1.44 \times 10^{-4}] \quad .$$

Hence, over the whole period of temperature measurements, the influence of the thermocouple leads is negligible.

McMahon also derived an expression for $\partial T_3/\partial t$, which is given by:

$$\frac{\partial T_3}{\partial t} = \frac{q}{\rho_3 C_3 b}\left[1 + \frac{a^2}{4\varkappa_1}\frac{\sqrt{\varkappa_2}}{b}\frac{1}{\sqrt{\pi}\,t}\left\{\frac{\Gamma'(1/2)}{\Gamma(1/2)} - \log\left(\frac{\varkappa_1 t}{a^2}\right)\right\}\right] \quad (C\text{-}10)$$

Again, in the absence of the wire, the expression would simply be:

$$\frac{\partial T_3}{\partial t} = \frac{q}{\rho_3 C_3 b} \quad . \quad (C\text{-}11)$$

Hence, the error is given by:

$$\varepsilon' = \frac{a^2}{4\varkappa_1}\frac{\sqrt{\varkappa_2}}{b}\frac{\rho_2 C_2}{\rho_3 C_3}\frac{1}{\sqrt{\pi t}}\left\{\frac{\Gamma'(1/2)}{\Gamma(1/2)} - \log\left(\frac{\varkappa_1 t}{a^2}\right)\right\} \quad . \quad (C\text{-}12)$$

If again it is assumed that the wire and sheet are of the same material, the error will be given by

$$\varepsilon' = \frac{a^2}{4\sqrt{\varkappa_1}}\frac{1}{b}\frac{1}{\sqrt{\pi t}}\left\{\frac{\Gamma'(1/2)}{\Gamma(1/2)} - \log\left(\frac{\varkappa_1 t}{a^2}\right)\right\} \quad . \quad (C\text{-}13)$$

Now, since $\sqrt{t}$ appears in the denominator, ε will have its maximum values for small t. Since during the experimental investigation reported here, temperatures were measured from t = 1 min. onwards, ε' is evaluated for t = 60 sec.

$$\varepsilon' \simeq -0.245 \times 10^{-4}$$

$$\therefore \; F(t) = \text{const.}\,[60 - 0.245 \times 10^{-4}]$$

$$= \text{const.}\,[1 - 4.1 \times 10^{-7}] \quad .$$

Again, the error is much less than 1 per cent.